Treball de Fi de Grau
Bachelor Final Thesis

Grau en Enginyeria de Tecnologies Industrials

Renewable Energy Microgrid:

Design and Simulation

Author: Jordi Sarradell Laguna
Director/Codirector: Oriol Gomis Bellmunt / Eduard Prieto Araujo

Dead Line: June 2017

ETSEIB

CITCEA UPC

UPC

Abstract

This project designs, models and simulates a microgrid with the next characteristics:

- Grid-connected
- Zero Net-Metering with the grid (Zero Energy Building concept)
- Low Voltage Direct Current (LVDC) distribution system
- Solar generation
- Storage system → battery
- Other components: loads, electrical vehicle…

This paper presents the basic theoretical principles and equations to model the main components of the system (PV panels, converters, control systems, etc) and displays the Simulink models of the different solutions found, and the graphical results obtained in the simulations.

The project also discusses some very innovative issues in the power systems panorama, as the LVDC distribution system and the zero-energy building concept.

Contents

1. Nomenclature

$I_{DC}\ [A] \rightarrow DC\ current\ of\ the\ DC\ bus$

$P_{VSC}[W] \rightarrow Power\ transfered\ in\ the\ VSC\ converter$

$E_{DC}^{*}\ [V] = 800V \rightarrow DC\ voltage\ reference\ of\ the\ DC\ bus$

$E_{DC}\ [V] \rightarrow DC\ real\ voltage\ of\ the\ DC\ bus$

$I_{abc}\ [A] \rightarrow AC\ current\ of\ the\ three-phase\ AC\ bus$

$V_{z,abc}[V] \rightarrow AC\ voltage\ of\ the\ three-phase\ utility\ grid$

$i_{qd0}\ [A] \rightarrow Park\ transformed\ AC\ currents$

$V_{z,qd0}\ [V] \rightarrow Park\ transformed\ AC\ utility\ grid\ voltage$

$V_{l,abc}[V] \rightarrow AC\ voltage\ of\ the\ three-phase\ VSC\ side$

$V_{l,qd0}[V] \rightarrow Park\ transformed\ voltage\ of\ the\ three-phase\ VSC\ side$

$[T_{qd0}] \rightarrow Park\ Transformation\ Matrix$

$i_q^{*}\ ,\ i_d^{*}\ [A] \rightarrow\ synchronous\ frame\ (Park)\ current$

$K_p\ , K_i\ [adim.] \rightarrow respectively, proportional\ and\ integral\ constants\ of\ PI\ controller$

$R\ [\Omega], L\ [H], C\ [F] \rightarrow respectively: resistance, iductance, capacitance$

$\tau\ [s] \rightarrow time\ constant\ in\ firs-order\ dynamic\ systems$

$w_e = 2\pi f_e\ [rad/s]\ , f_e = 50\ Hz \rightarrow respectively: electrical\ angular\ velocity\ and\ frequency$

$P^{*}[W], Q^{*}[var] \rightarrow active\ and\ reactive\ power\ references$

$P\ [W], Q[var] \rightarrow active\ and\ reactive\ real\ power$

$\xi\ , w \rightarrow respectively, dumping\ ratio\ and\ natural\ angular\ vel. of\ a\ second-order\ system$

$I_{ph}[A] \rightarrow Photo-generated\ current$

$I_d[A] \rightarrow Diode\ current$

I_o , $I_{o,ref}[A] \rightarrow respectively, real\ and\ reference\ inverse\ saturation\ current\ of\ the\ diode$

$I_{sh}[A] \rightarrow current\ (losses)\ in\ the\ shunt\ resistance$

$G, G_{ref}[W/m^2] \rightarrow respectively, real\ and\ reference\ irradiance$

$I_{sc}[A], V_{oc}\ [V] \rightarrow respectively, short-circuit\ current\ and\ open-circuit\ voltage$

$K_{ti}\ [A/K]$, $K_{tv}[V/K] \rightarrow respectively, temperature\ coefficients\ for\ I_{sc}\ and\ V_{oc}$

T_c , $T_{c,ref}[K] \rightarrow respectively, real\ and\ reference\ cell\ operation\ temperatures$

$\eta\ [adim.] \rightarrow ideality\ factor\ of\ the\ diode$

$V_t[V] \rightarrow temperature\ equivalent\ voltage$

$\sigma = 1.38065 \cdot 10^{-23}\ J/K \rightarrow Boltzmann\ constant$

$e = 1.60217\ C \rightarrow charge\ of\ an\ electron$

$E_g = 1.12\ eV \rightarrow Gap\ Energy\ (Silicon)$

R_s , $R_{sh}[\Omega] \rightarrow respectively, series\ and\ shunt\ resistance$

$(I_{mp}, V_{mp}) \rightarrow maximum\ power\ point\ (MPP)$

$P_{mp}[W] \rightarrow maximum\ power$

m_p , $m_s \rightarrow respectively, paralel\ ans\ series\ connected\ PV\ modules\ in\ a\ PV\ array$

$D \rightarrow duty\ cycle\ of\ the\ converter$

$SOC\ [\%] \rightarrow State\ Of\ Charge\ of\ the\ battery$

2. Preface

2.1. Origin of the project and motivations

This project is the culmination of other previous similar projects which I have been developing during the last year.

My first approach to the microgrids and the renewable energy generation systems was in February 2016, when I started a project tutored by the professor Oriol Gomis Bellmunt which consisted in the design and sizing of an autonomous microgrid based in eolic generation and a pump-turbine hydroelectric storage system in an isolated island called Brava (located in the Cabo Verde archipelago). This project was a good way to get myself introduced into this complex field, but it wasn´t as detailed as I would like in the technical aspects.

A few months later, in August 2016, I started an ERASMUS+ mobility program and I moved to the Netherlands in order to study in TU Delft during six months. During my stay there, I started a group project about modeling an autonomous solar powered microgrid for 50 households and simulate its behavior under different conditions. That project was my first approach to simulations of power systems using the *Matlab-Simulink* software package. While I was doing that project I realized that my interest in this technology was increasing, and I decided to contact Oriol Gomis again and request him to be the tutor of my Bachelor final thesis.

The motivation was to get into detail about the converters and control systems needed for the correct modeling of a feasible grid-connected microgrid.

2.2. Definition of the problem and Objectives

The main objective of this project is to find a solution for the next problem: design a microgrid for a grid-connected, Zero-Energy Building, with a Low Voltage Direct Current (LVDC) distribution system, photovoltaic distributed generation, and a suitable storage system.

2.3. Scope

In Scope:

- Design the general scheme of the microgrid
- Identify all its components
- Model and simulate the principal components acting independently
- Simulation of the solar generation and the storage system
- Describe the required converters
- Simulate the average model of the converters
- Describe (qualitatively) the required controls to get Zero Net-Metering

Out of scope:

- Simulation of the entire microgrid during a long period of time
- Taking into account commutation losses or converter efficiencies
- PWM controllers for the converters
- Economic and environmental impact
- Doing an accurate study of the electrical demand in the building
- Placing the microgrid in a real territory

2.4. Required knowledge and skills

Knowledge in:

- Electrical Engineering
- Dynamical systems and PI controllers
- Solar cells and arrays
- Power electronics and converters
- Power systems

Skills:

- “Matlab/Simuling” software package

3. Introduction and State of the Art

References for this section:

- "Nuevo Modelo de distribución de corriente continua en baja tensión en Smart Buildings"- Authors: Luis Hernández Callejo, Yolanda Estepa Ramos, Guillermo Martínez de Lucas – Universidad Politécnica de Madrid (UPM) in collaboration with Universidad de Zaragoza and CIEMAT [1]
- "An LVDC Distribution System Concept" – Authors: Pasi Salonen, Tero Kaipia, Pasi Nuutinen, Pasi Peltoniemi, Jarmo Partanen – Lappeenranta University of Tecnology, Sweden [2]
- "Possibilities of the low voltage DC distribution systems" – Authors: Tero Kaipia, Pasi Salonen, Jukka Lassila, Jarmo Partanen – Lappeenranta University of Technology, Sweden [3]

3.1. Microgrids and Renewable Energy

Microgrids are electricity distribution systems containing loads and distributed energy resources, (such as distributed generators, storage devices, or controllable loads) that can be operated in a controlled, coordinated way either while connected to the main power network or while islanded.

Due to the latest developments of renewable (solar, wind, biomass, etc) distributed generation systems, microgrids have been becoming more important because of its possible applications in powering isolated areas or autonomous systems.

The main benefits of renewable generation are, of course, environmental. Reducing CO_2 and other greenhouse gases emissions to the atmosphere is one of the main objectives and responsibilities of our generation.

Distribution Energy Resources (DER) are decentralized, modular and more flexible technologies that are located close to the load they serve (local, small-scale). Due to the irregularity of the Renewable sources (sun irradiance, wind speed), microgrids require special storage systems to store energy and give it to the system when required.

In this project the main essential components of a renewable microgrid are studied and simulated.

3.2. LVDC Distribution System Concept

The demand for undisturbed electricity is growing while society relies more and more on electricity. The occurring outages have more effects to the customers and outage costs increases. At the same time the climate is changing and causing bigger storms than before. The network disturbances caused by storms have become larger and the number is increased. These challenges have raised demand for more reliable network solutions compared to traditional 20/0.4 kV 3-phase AC distribution systems. The LVDC distribution system concept responds to these challenges in field of electricity distribution.

Today's utilization of DC technology concentrates mainly to HVDC transmission systems, industrial distribution and electric drives. But from technological point of view the DC distribution system is a new concept in electrical distribution and it generates a new area of business to power electronic device manufacturers.

Low voltage direct current distribution can be an adequate technology for smart grids and microgrids because currently some of the renewable sources generate DC current, principally photovoltaic panels. This energy can't be directly injected to the grid, it has to be transformed to AC current with inversors (current distribution systems are in AC).

LVDC distribution can be implemented in two different ways: wide distribution and link distribution:

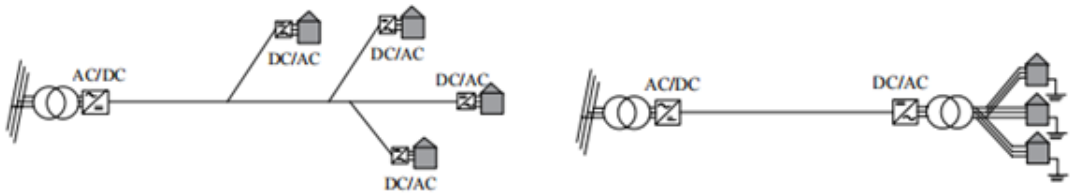

Fig. 3.1. Left, wide LVDC distribution. Right, Link LVDC distribution. Image extracted from "An LVDC Distribution System Concept" [2]

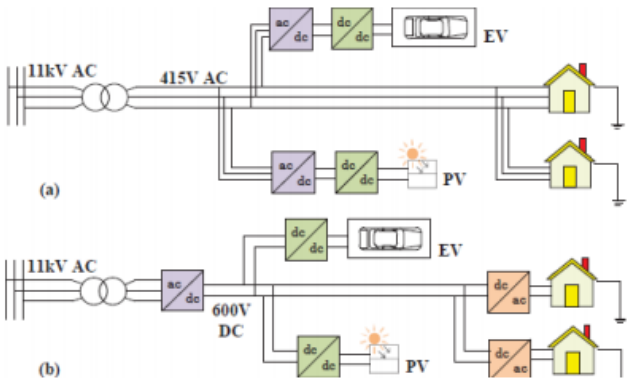

Fig. 3.2. (a) traditional distribution system against (b) possible LVDC distribution system for a Smart Building. Image extracted from "Nuevo modelo de distribución de corriente continua en baja tensión en Smart Buildings"[1]

- Benefits and challenges:

  Benefits:

  - Higher transmission capacity than traditional 400 VAC system resulting from the voltage difference between the systems.
  - The voltage quality also improves resulting from inverter's active voltage control.
  - Smaller currents and smaller power losses if the cables sizes are same in both systems, and the distribution line is shorter than 1.5 km. (figure 3.3)

  Challenges:

  - The DC system is more complex than traditional 20/0.4 kV AC distribution system which makes system operation more difficult.
  - Challenges to electrical safety: high earth voltages in difficult grounding condition.
  - Lifetimes of power electronic device may be only a quarter than traditional ones. Short lifetimes emphasize maintenance issues and costs of converters.

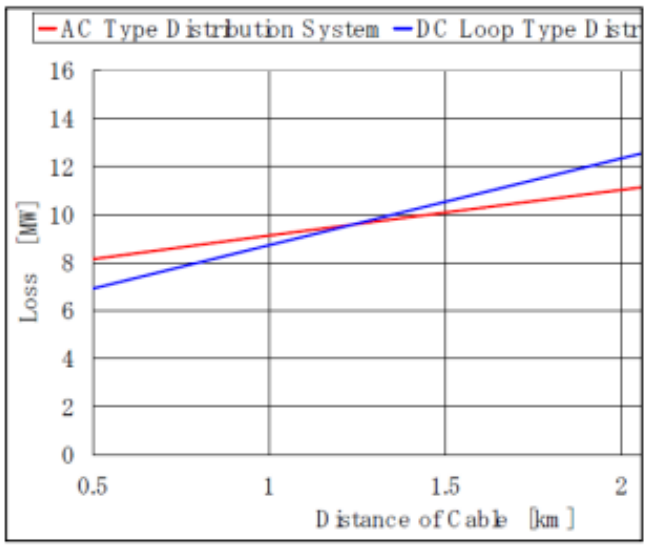

Fig. 3.3. Power losses in the cables depending on its length. Image extracted from "Nuevo modelo de distribución de corriente continua en baja tensión en Smart Buildings"[1]

- Current LVDC cases:

  Stroomversnelling is a Swedish project whose objective is creating zero-energy households, which are centralized in a LVDC distribution system. The electrical outlets are directly in DC and are based in USB, as shown in Figure 3.4.

  Stadskanaal (The Netherlands) will be the first town in the world with a LVDC distribution smart grid public lighting.

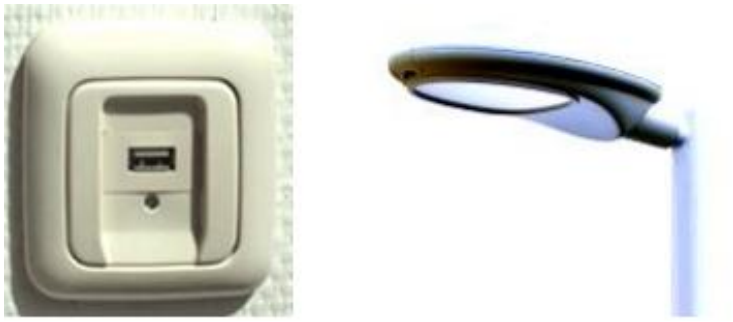

Fig. 3.4. Left, USB DC electrical outlet. Right, LED public lighting form Stadskanaal. Image extracted from "Nuevo modelo de distribución de corriente continua en baja tensión en Smart Buildings"[1]

3.3. Net Metering related with the Zero-Energy Building Concept

Net metering (or net energy metering, NEM) allows consumers who generate some or all of their own electricity to use that electricity anytime, instead of when it is generated. This is particularly important with wind and solar, which are non-dispatchable. Monthly net metering allows consumers to use solar power generated during the day at night, or wind from a windy day later in the month.

Provide that the Net-Metering of a building is zero. The building is not consuming power from the main grid, and that introduces the concept of Zero Energy Building, or Almost Zero Energy Building.

This project tries to achieve this objective, create the required controls in order to make the Net-Metering of the microgrid be zero.

4. Design of the system

4.1. General scheme and explanation of the system

The general system (microgrid) consists in the next components, all connected as showed in Figure 4.1.

1. Utility Grid
2. Three-Phase + Neutral AC bus
3. VSC Voltage Regulator converter connect to a DC bus
4. Three-Phase + *Single-Phase AC Loads
5. DC Distribution Bus
6. PV Array connected to the DC bus through DC/DC boost converter with MPPT control techniques
7. Battery connected to the DC bus through a bidirectional DC/DC buck-boost converter
8. Diesel Generator connected to the AC bus
9. Electrical Vehicle Charger connected to the DC bus through a DC/DC Buck converter
10. DC loads connected to the DC bus through a DC/DC buck converter
11. High level controller: reference controller + zero net-metering controller

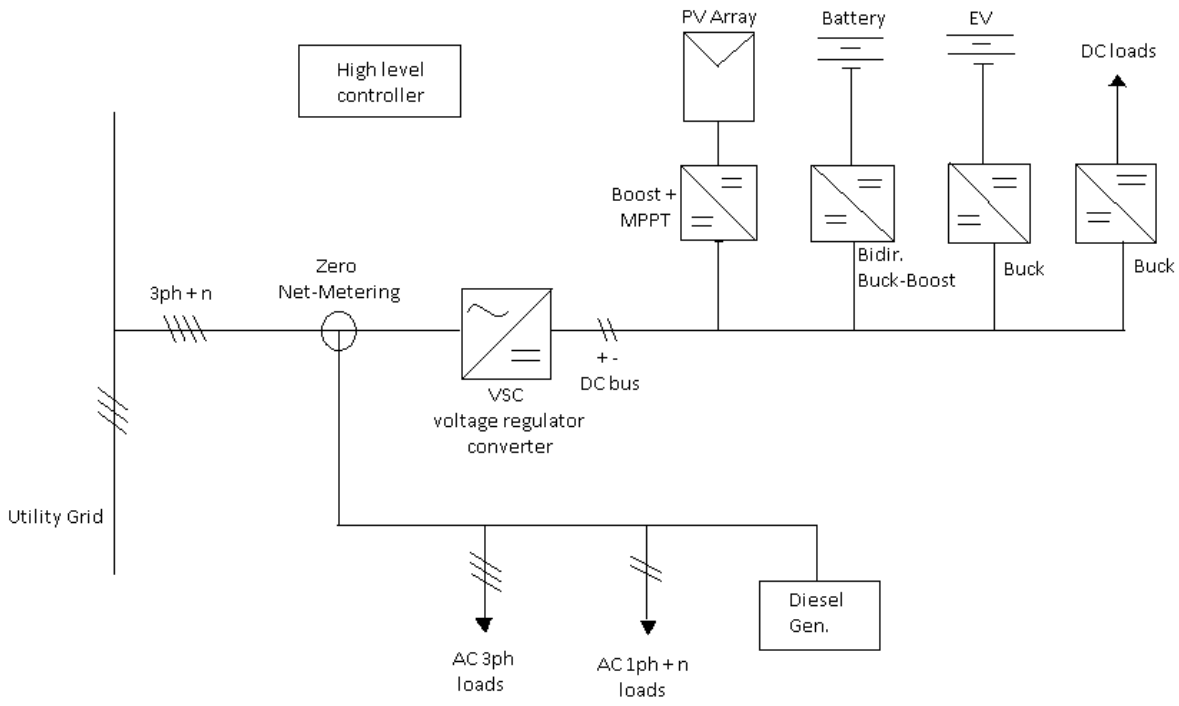

Fig.4.1. General scheme of the microgrid.

- Hypothesis and model considerations:

  In order to simplify the simulations, some hypothesis have been taken:

  1. EV Charger, Diesel Generator and DC loads haven't been modeled
  2. All the AC loads have been modeled as three-phase loads in order not to model the neutral phase
  3. The utility grid has been modeled as an ideal three-phase voltage source generator with $V_{peak} = \frac{400\sqrt{2}}{\sqrt{3}} V$ and $f_e = 50\ Hz$

4.2. Components

In this section all the components involved in the system are explained and discussed. For every single component, a theoretical explanation is provided and the equivalent model is explained and justified, showing its results.

4.2.1. VSC Voltage Regulator AC/DC bidirectional converter

This component has been modeled following the academic article "Active and reactive power control of grid connected distributed generation systems" by Agustí Egea Alvarez, Adrià Junyent Ferré and Oriol Gomis Bellmunt [4]

The function of this converter is to control the DC bus voltage and stabilize it to a reference constant value (regardless of the DC current) in order to guarantee power balance.

- Electrical description of the system:
  The AC side of the converter is connected to the utility grid (simplified Thévenin equivalent consisting in AC three-phase voltage source with resistive-inductive impedance connected in series) by three inductances (one connected to each phase). The DC side of the converter is connected to a DC bus, which has a controllable current source in order to simulate fluctuations in the DC current. The DC bus has a capacitance connected in parallel (shunt capacitor).

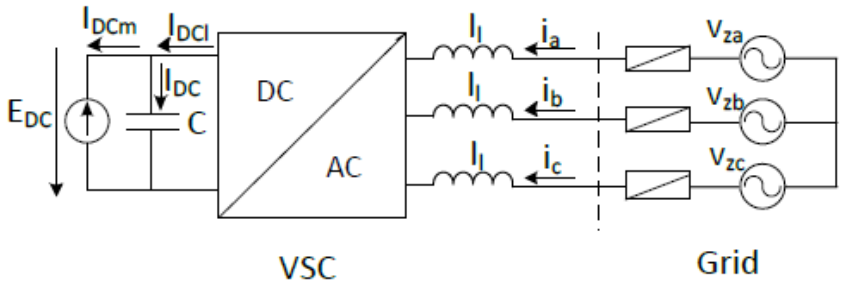

Fig.4.2. VSC converter with the DC side modelled as a current source and a shunt capacitor. Image extracted from "Active and reactive power control of grid connected distributed generation systems"[4]

- Electrical/Electronic description of the converter:

  The converter is composed of three branches with two Isolated Gate Bipolar Transistors (IGBTs). The middle point of each branch is smoothly connected to one different phase of the grid by means of inductances. Antiparallel diodes are connected to the IGBTs in order to prevent the system from extremely high overshoots in the voltage of the transistors produced by the inductances when they react to high current derivatives.

  The commutation cycle (PWM) of the IGBTs is not described because it's not necessary for our model.

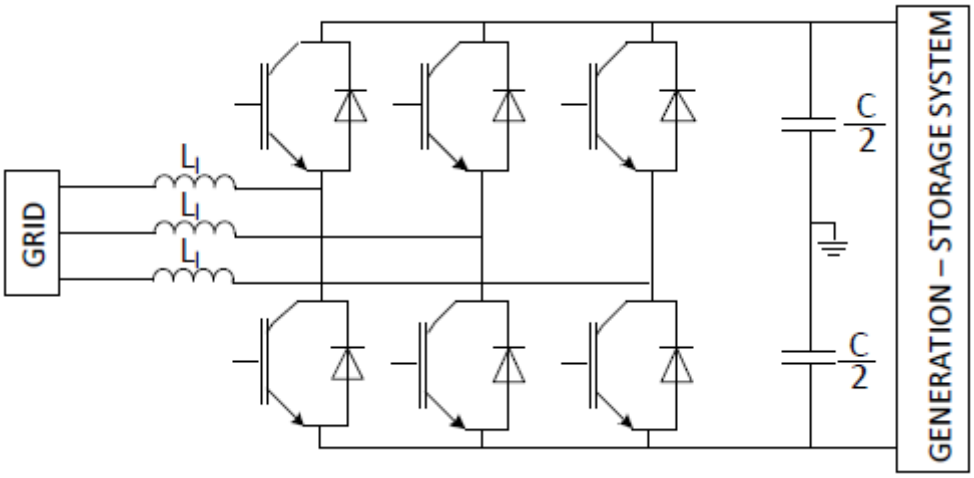

Fig.4.3.Electrical components and distribution of the VSC converter. Image extracted from "Active and reactive power control of grid connected distributed generation systems" [4]

- Description of the average model:

  The transistors are not modelled in the model used for this project. The model only works with the average power so the commutation losses in the IGBTs are neglected. Because of this reason, the PWM control for the transistors is not necessary. This kind of models are a simplification of the reality, but they are very computational efficient and practical (especially when they are used in a bigger model)

  The model consists of two subsystems: the power subsystem and the control subsystem (As seen in figure 4.4)

  - The power subsystem is directly connected to the AC and DC part and receives inputs from the control subsystem to make its function.
  - The control subsystem receives the control signals from the user and inputs from the grid and computes the proper values, which are sent to the power subsystem to be executed.

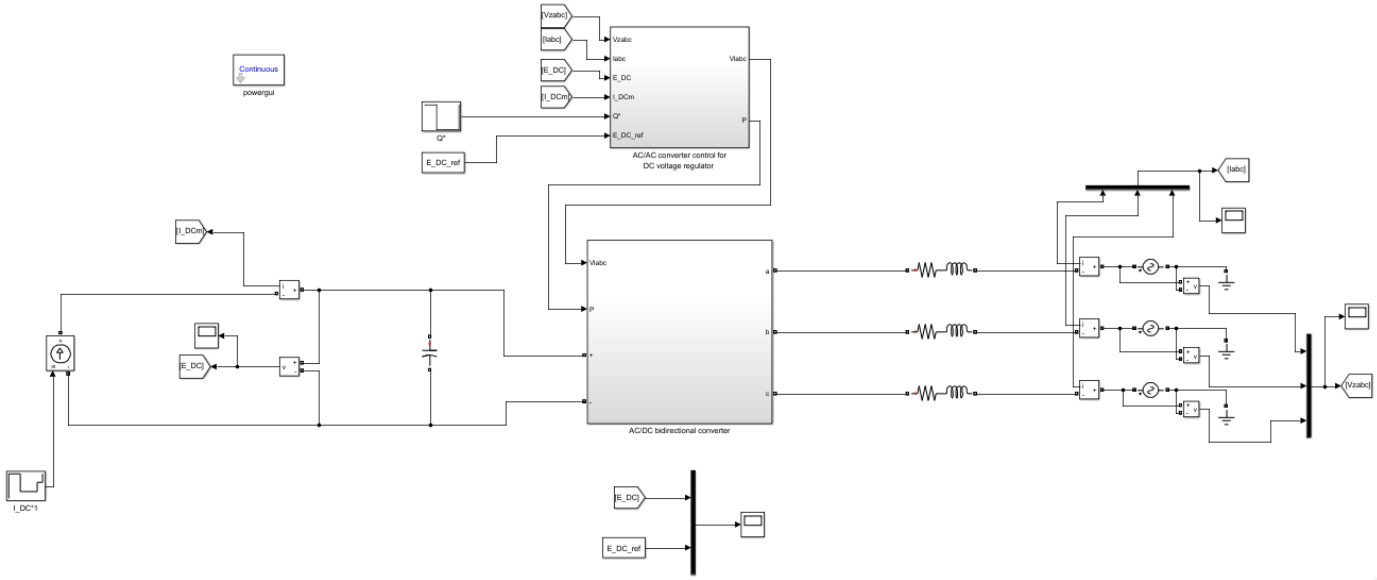

Fig. 4.4. Average model for the VSC converter. The right part simulates the utility grid, the left part is the DC bus whose voltage is being controlled, the central block is the Power subsystem and the block on the top is the Control subsystem. Produced by tha author with "Matlab/Simulink"

- Power subsystem: (Figure 4.5)

  The AC part of the power subsystem consist of three controlled AC voltage sources (one connected to each phase) which will operate at variable voltages. The computation and control of these voltages will be explained later.

  The DC part consists of one controllable DC current source which will satisfy this equation:

$$I_{DC} = \frac{P_{VSC}}{E_{DC}^*} \;;\; E_{DC}^* = 800V \; (eq.1)$$

  Being P_{VSC} the power transferred from the AC part to the DC part and being E_{DC}^* the voltage reference (which will be imposed to the DC bus).

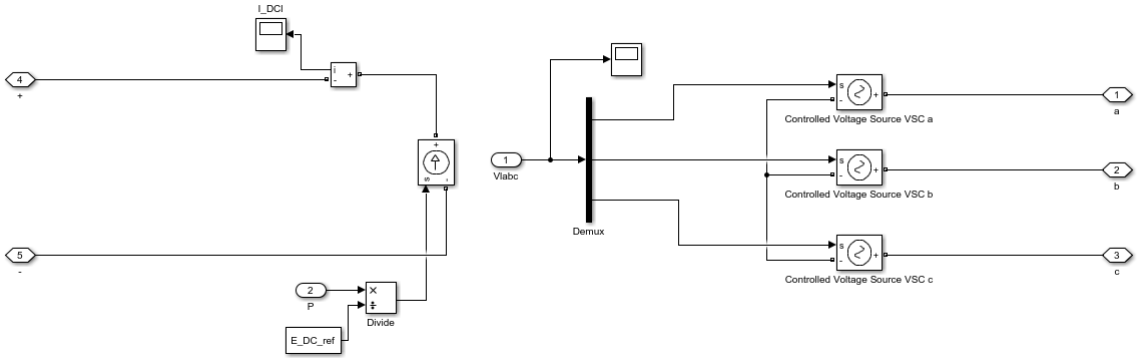

Fig. 4.5. Average model for the power subsystem. AC part modeled with three controllable AC voltage sources and DC part with one controllable DC current source. Produced by the author with "Matlab/Simulink"

- General control Scheme (Figure 4.6):
  1) I_{abc} , $V_{z,abc}$ transformed to i_{qd0} , $V_{z,qd0}$ with the Park transformation
  2) V_{qd0} goes into a Phase Locked Loop (PLL) → $V_{zd} = 0$ and electrical angle of the grid is tracked (θ)
  3) Reference computation: the required references are computed i_q^* , i_d^*
  4) Current loop control: the required values for V_{lq} , V_{ld} are computed.
  5) V_{lq} , V_{ld} transformed to $V_{l,abc}$ with the inverse Park transformation and sent to the power subsystem

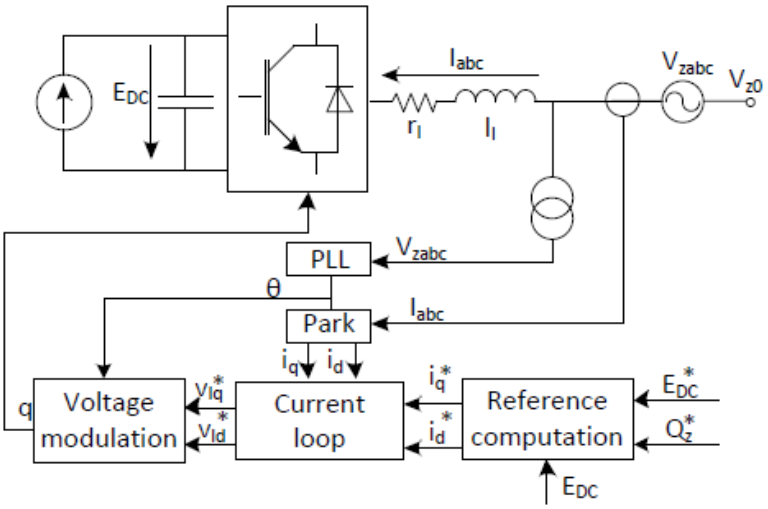

Fig. 4.6. Visual explanation of the general control scheme of the control subsystem. It is important to remark that the block "voltage modulation" will not be implemented in the average model because it´s not necessary to simulate the commutation of the IGBTs. Image extracted from "Active and reactive power control of grid connected distributed generation systems" [4]

- Park Transformation: Mathematical transformation which transforms a three-phase sinusoidal signal to a constant value equivalent to the peak value of the sinus, after a few short ramp transient. This transformation extremely simplifies the control of three-phase voltages and currents.

$$[x_{qd0}] = [T_{qdo}]\,[x_{abc}]\ (eq.2)$$

and its inverse,

$$[x_{abc}] = [T_{qdo}]^{-1}[x_{qd0}]\ (eq.3)$$

With transformation matrices:

$$T(\theta) = \frac{2}{3}\begin{bmatrix} \cos(\theta) & \cos\left(\theta - \frac{2\pi}{3}\right) & \cos\left(\theta + \frac{2\pi}{3}\right) \\ \sin(\theta) & \sin\left(\theta - \frac{2\pi}{3}\right) & \sin\left(\theta + \frac{2\pi}{3}\right) \\ 1/2 & 1/2 & 1/2 \end{bmatrix} (eq.4)$$

and its inverse,

$$T^{-1}(\theta) = \frac{2}{3}\begin{bmatrix} \cos(\theta) & \sin(\theta) & 1 \\ \cos\left(\theta - \frac{2\pi}{3}\right) & \sin\left(\theta - \frac{2\pi}{3}\right) & 1 \\ \cos\left(\theta + \frac{2\pi}{3}\right) & \sin\left(\theta + \frac{2\pi}{3}\right) & 1 \end{bmatrix} (eq.5)$$

Where the parameter θ is the instantaneous electrical angle of the first phase A, which will be computed in the Phase Locked Loop (PLL)

This transformation can also be analyzed graphically as a transformation in the α, β plane (Clark transformation, which is not explained in this report) plus a θ rotation, as illustrated in figure 4.7

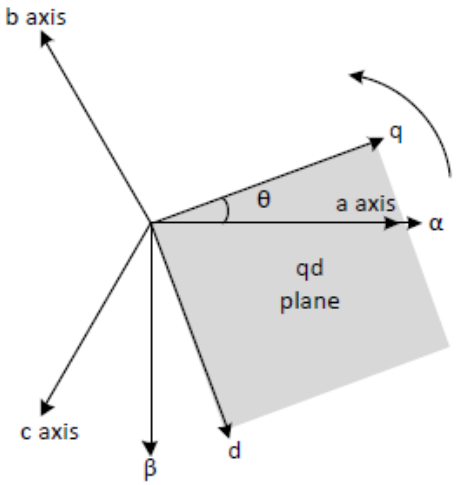

Fig. 4.7. qd plane representation. Image extracted from "Active and reactive power control of grid connected distributed generation systems" [4]

- Phase Locked Loop:

  This element has two main functions:

  - Determine the angle and the angular velocity of the electrical network (θ and ω, respectively)
  - Stabilize $V_{z,d}$ to zero

  It consists in a feedback of $V_{z,d}$ filtered by a PI controller with a 0 reference. The output of this PI controller is the electrical angle θ, which can be integrated to obtain the angular velocity ω (Figure 4.8)

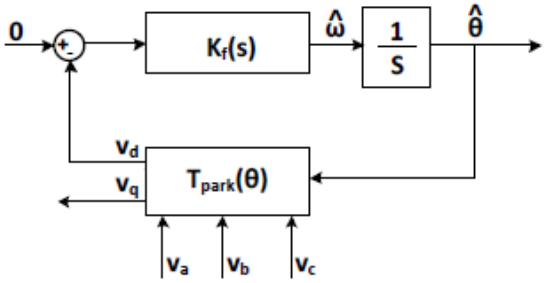

Fig. 4.8. Typical PLL scheme. Image extracted from "Active and reactive power control of grid connected distributed generation systems" [4]

It can be observed that for computing the Park transformation the electrical angle θ is required, and for computing the electrical angle θ, the Park transformation is required. This is the typical scheme of a system which needs feedback to be solved. These type of systems are solved numerically in an iterative way.

Equations for the PI controller are:

$$K_f(s) = \left(K_{p,PLL} + \frac{K_{i,PLL}}{s}\right) + w_e \ (eq.6)$$

$$K_{i,PLL} = {}^{1}/_{\tau_{PLL}} \ (eq.7)$$

$$w_e = 2\pi f_e \ (eq.8)$$

Where K_p is the proportional gain, K_i is the integrator gain, w_e is the angular velocity, τ_{PLL} is the time constant of the PLL and $f_e = 50\ Hz$ is the oscillating frequency of the grid voltage source.

The optimal sizing of the PI controller for this PLL is completely out of the scope of this project, so $K_{p,PLL} = 1$ and $\tau_{PLL} = 10^{-3}$ have been considered reasonable values.

After the Park transformation and the PLL controller, the voltages are transformed as illustrated in Figure 4.9:

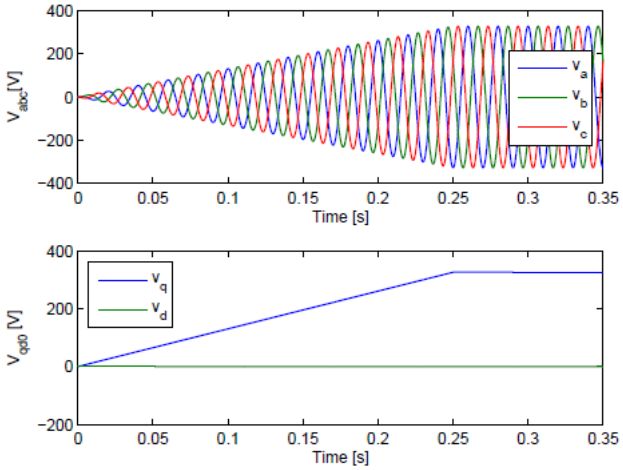

Fig. 4.9. On the top, three-pase grid voltages in abc frame. On the bottom, three phase grid voltages in qd0 frame. Notice that Vd is forced to zero. Notice that there is a short transient of 0.25s aproximately. Image extracted from "Active and reactive power control of grid connected distributed generation systems" [4]

- Reference computation:

Instantaneous power theory on synchronous frame (qd frame) shows that the active and reactive power equations are: (notice that $V_{z,d} = 0$)

$$P = \frac{3}{2}\left(V_q i_q + V_d i_d\right) = \frac{3}{2} V_q i_q \ (eq.9)$$

$$Q = \frac{3}{2}\left(V_q i_d + V_d i_q\right) = \frac{3}{2} V_q i_d \ (eq.10)$$

Being P^* and Q^* the active and reactive power references, the qd current references can be computed as:

$$i_q^* = \frac{2}{3}\frac{P^*}{V_{z,q}} \ (eq.11)$$

$$i_d^* = \frac{2}{3}\frac{Q^*}{V_{z,q}} \ (eq.12)$$

But the active power reference is not a direct reference. The only direct references of the system are the reactive power reference and the DC voltage reference, so it is necessary to compute P^* with a feedback PI controller, as illustrated in the diagram of Figure 4.10.

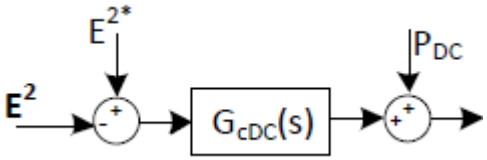

Fig. 4.10. Feedback PI Voltage controller for the computation of the active power reference. Image extracted from "Active and reactive power control of grid connected distributed generation systems" [4]

$$P^* = P_C^* + P_{DC}\ (eq.13)$$

$$P_{DC} = E_{DC} I_{DC_m}\ (eq.14)$$

$$P_C^* = G_{cDC}(s)(E_{DC}^{*2} - E_{DC}^2(s))\ (eq.15)$$

$$G_{cDC}(s) = K_{p,DC} + \frac{K_{i,DC}}{s}\ (eq.16)$$

$$K_{p,DC} = C\xi_{DC}\omega_{DC}\ (eq.17)$$

$$K_{i,DC} = \frac{C\omega_{DC}^2}{2}\ (eq.18)$$

Where P_C^* is the power injected to the capacitor, P_{DC} is the power in the DC bus (before the capacitor), I_{DCm} is the current in the DC bus (before thje capacitor), C is the capacitance of the capacitor and (ξ_{DC}, ω_{DC}) are, respectively, the dumping ratio and the angular velocity that describe the second-order dynamics of the DC voltage. This two last parameter are design parameters, they can be modified in order to have different dynamics for the loop (quicker stabilization, smaller overshoot, etc.)

In this case: $C = 1020\mu F$, $\xi_{DC} = 0.707$, $\omega_{DC} = 418.88\, rad/s$

- Current loop control:

  This is the final step of the control scheme. This control loop computes the required $V_{l,q}$, $V_{l,d}$ that need to be forced into the VSC three-phase voltage sources (AC sides) in order to reach the current references i_q^* , i_d^* computed before (reference computation).

  Voltage equations:

$$\begin{bmatrix} V_{z,q} \\ 0 \end{bmatrix} - \begin{bmatrix} V_{l,q} \\ V_{l,d} \end{bmatrix} = \begin{bmatrix} R & L\omega_e \\ L\omega_e & R \end{bmatrix} \begin{bmatrix} i_q \\ i_d \end{bmatrix} + \begin{bmatrix} L & 0 \\ 0 & L \end{bmatrix} \frac{d}{dt} \begin{bmatrix} i_q \\ i_d \end{bmatrix} \quad (eq.19)$$

  Where R and L are, respectively, the resistance and inductances of the grid and the AC part of the converter.

  In equation 19 it can be observed that q and d components of voltages and currents are coupled. In order to control both components independently they have to be decoupled as illustrated in figure 4.11 (decoupling variables in controllable multivariable systems is a complex approach in automatic control engineering which is not going to be deeply explained in this report, so only the solution is showed)

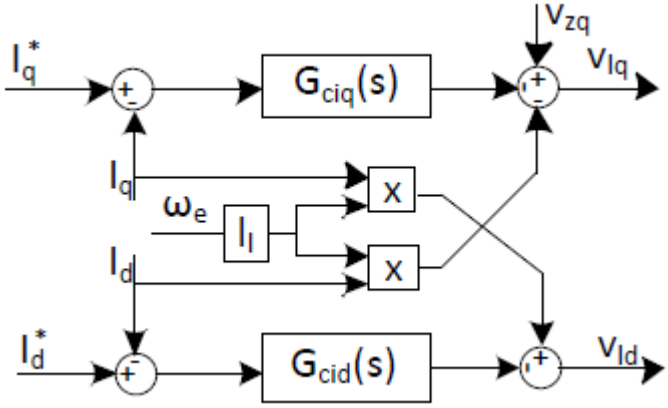

Fig. 4.11. Current controller decoupling and controlling iq and id separately. Image extracted from "Active and reactive power control of grid connected distributed generation systems" [4]

$$G_{c,iq}(s) = G_{c,id}(s) = K_p + \frac{K_i}{s} \quad (eq.20)$$

$$K_p = {}^{L}/_{\tau} \quad (eq.21)$$

$$K_i = {}^{R}/_{\tau} \quad (eq.22)$$

Where τ is the time constant of the first-order dynamics of the electrical system. When the references (i_q^* , i_d^*) instantaneously change their value (step), it takes τ seconds to the real currents (i_q , i_d) to reach the 63% of that value. So, τ is a design parameter that models the response speed. In this case: $R = 0.5\ \Omega$, $L = 5.4\ mH$, $\tau = 10^{-3}$

- Control subsystem:

  The control subsystem consists of five main blocks, implemented with the equations exposed in the previous sections:

  - Park transformation (Figure 4.12)
  - Park inverse transformation (Figure 4.13)
  - Reference Computation (Figure 4.14)
  - Phase Locked Loop (PLL) (Figure 4.15)
  - Current control loop (Figure 4.16)

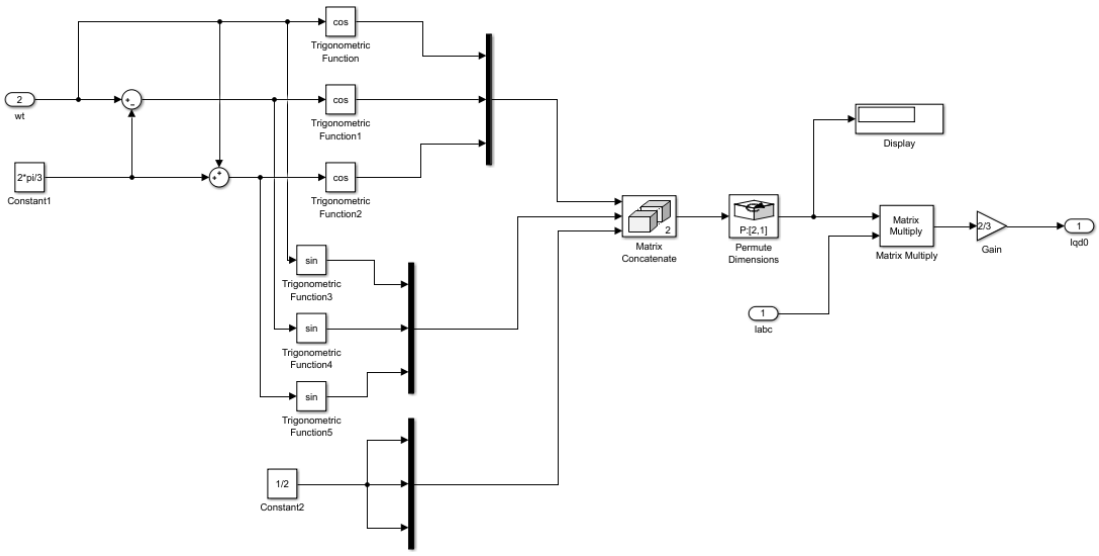

Fig. 4.12. transformation, following equations 2,4. Produced by the author with "Matlab/Simulink"

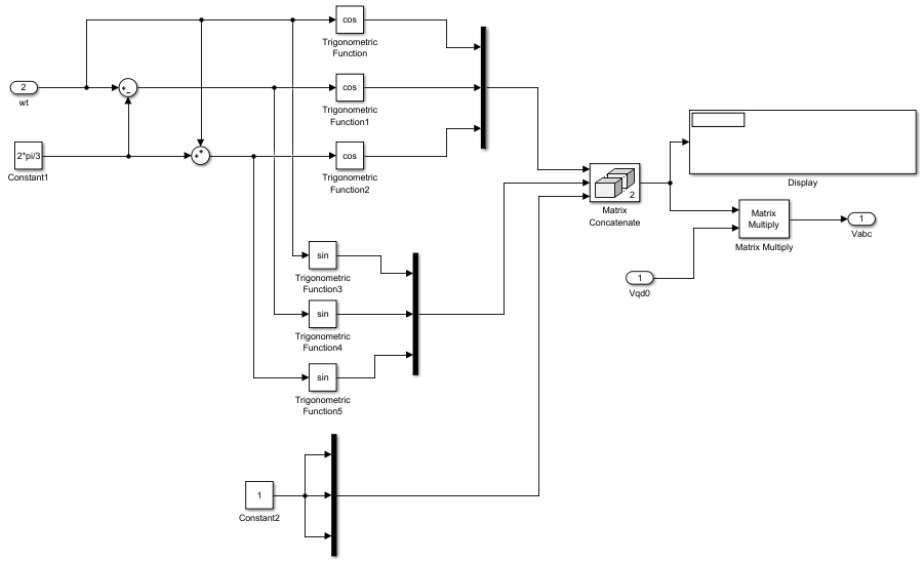

Fig. 4.13. Block implemented inverse Park transformation, following equations 3,5. Produced by the author with "Matlab/Simulink"

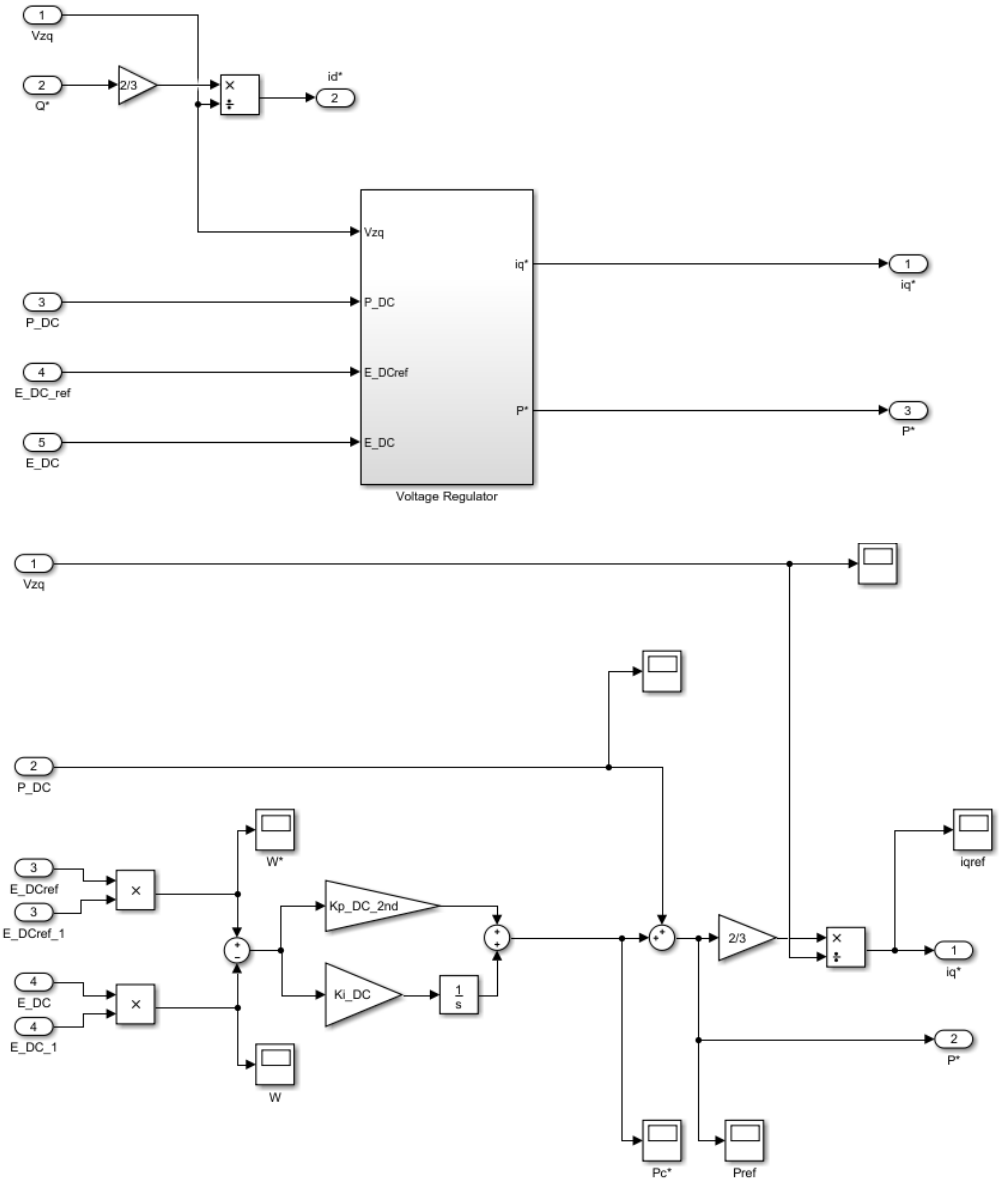

Fig. 4.14. Block implemented Reference Computation system (On the bottom, Voltage Regulator where the active power reference is computed and the second order dynamics is imposed to the DC voltage) , following equations 11,12,13,14,15,16,17,18. Produced by the author with "Matlab/Simulink"

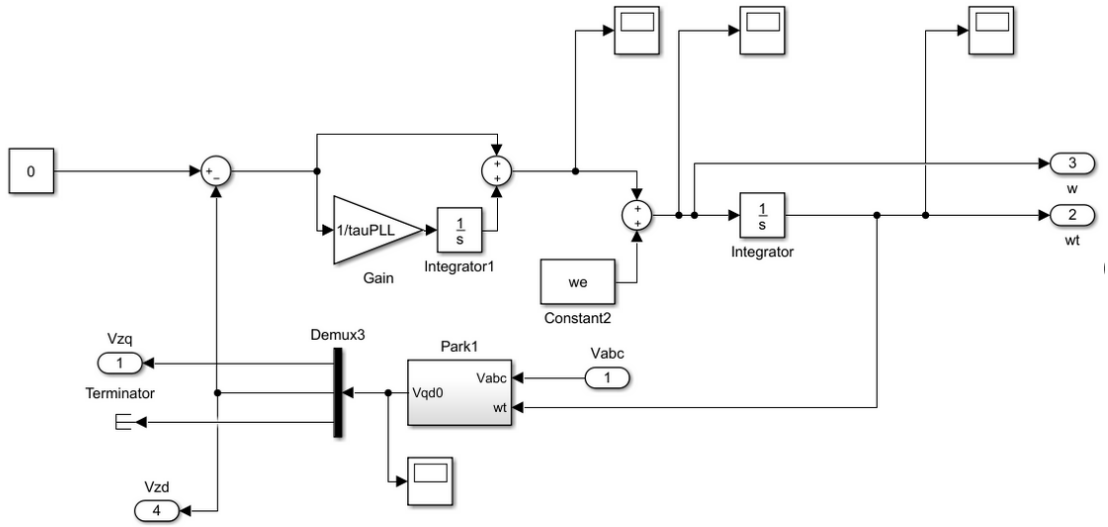

Fig. 4.15. Block implemented PLL system (with Park transformation block in it giving feedback to the PI controller) , following equations 6,7,8. Produced by the author with "Matlab/Simulink"

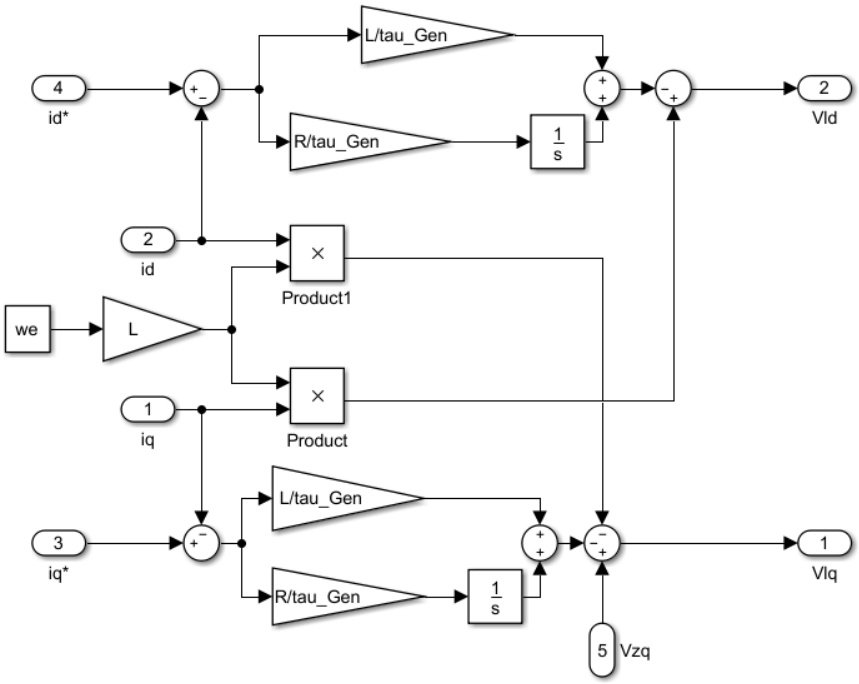

Fig. 4.16. Block implemented Current Control system (qd currents are controlled to their references with a first-order dynamics and AC voltages for the VSC voltage sources are computed) , following the equivalent decoupled equation of the equation 19 and equations 20,21,22. Produced by the author with "Matlab/Simulink"

- Results:

The most relevant results are showed and analysed in this section under this three direct references:

- $E_{DC}^{*} = 800\ V$
- Q^{*} is a stair reference signal with thie next values:

- $I_{DC,m}$ is a stair reference signal with the next values:

- DC Bus Voltage:

In Figure 4.17 it can be observed that the control subsystem stabilyzes the DC bus voltage (E_{DC}) to the reference value $E_{DC}^{*} = 800\ V$ every time there is a step in the DC current of the bus.

If the image is zoomed (Figure 4.18) the dynamics of the system can be clearly apreciated.

- The DC voltage takes approximately 22.54 ms to get the reference value
- It has a maximum relative overshoot (refered to the DC current step) of:

$$\frac{\left|E_{DC,max} - E_{DC}^{*}\right|}{\left|\Delta I_{DC,m}\right|} \cong 0.443\ {}^{V}/_{A}$$

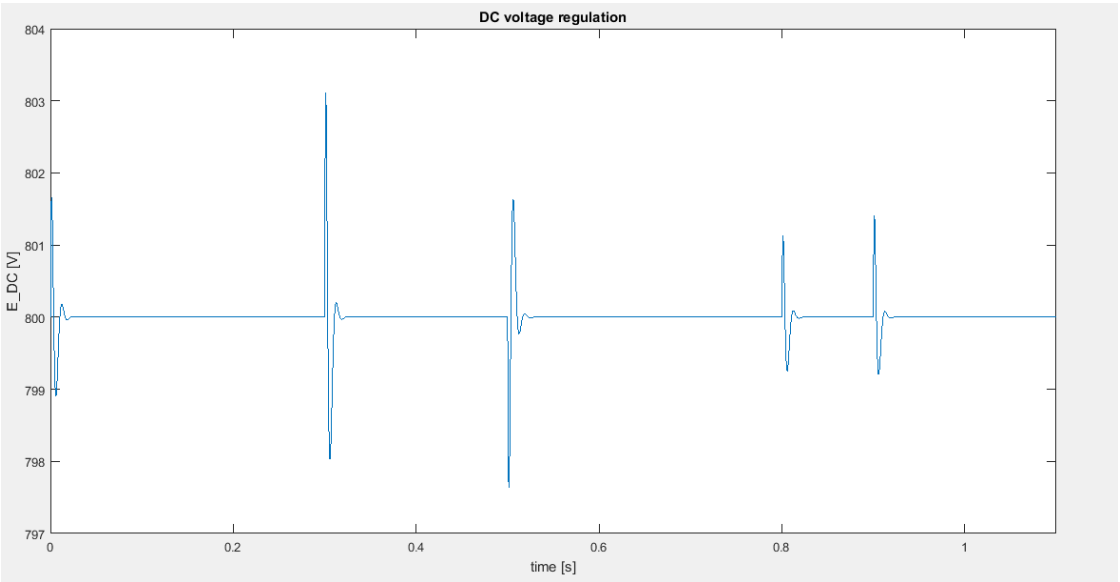

Fig. 4.17. DC Voltage Regulation. Produced by the author with "Matlab/Simulink"

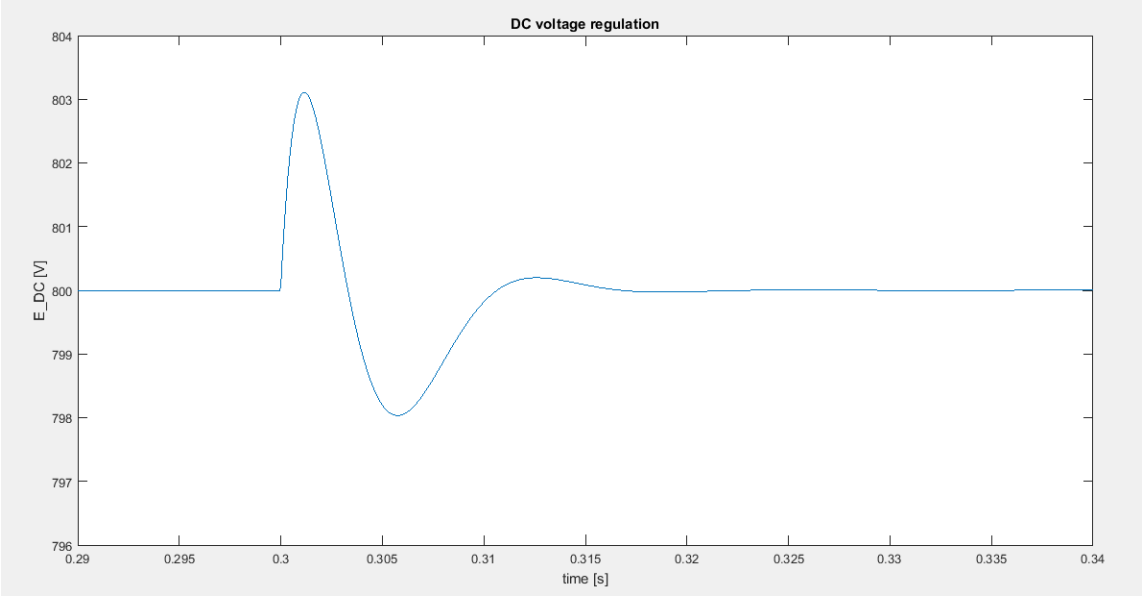

Fig. 4.18. Detailed DC Voltage Regulation. Produced by the author with "Matlab/Simulink"

- qd frame VSC voltages ($V_{l,q}$, $V_{l,d}$) and qd frame grid voltages ($V_{z,q}$, $V_{z,d}$)
  The grid voltages are constant and the VSC voltages change every time that there is a step in the DC current reference or the reactive power reference. (Figure 4.19)
  It can be observed that:
  - $V_{z,q} = V_{peak} = \frac{400\sqrt{2}}{\sqrt{3}} = 326.6\ V$ (amplitude of the grid voltage)
  - $V_{z,d} = 0\ V$ (because of the PLL controller)

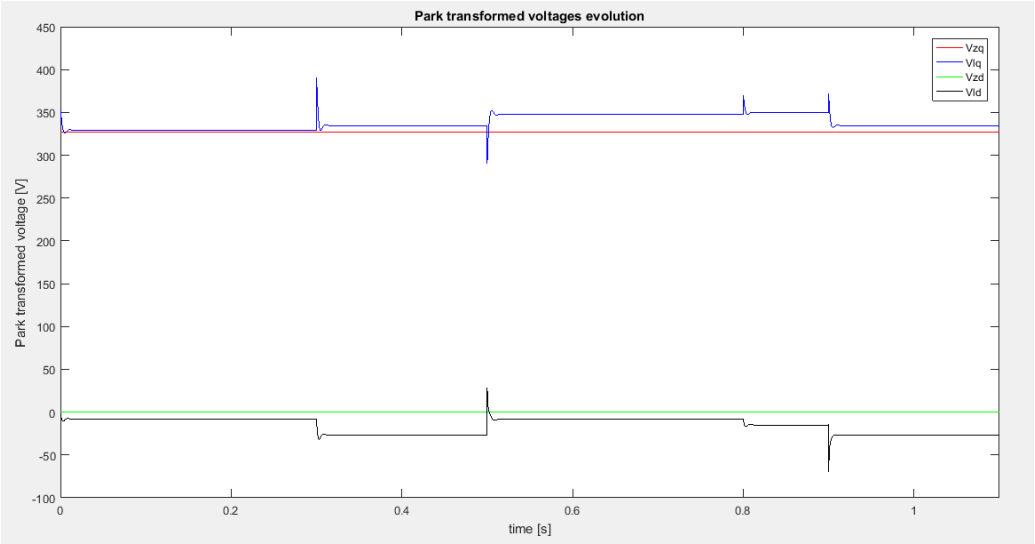

Fig. 4.19. synchronous frame voltages (VSC and Grid). Produced by the author with "Matlab/Simulink"

- qd frame VSC real currents (i_q, i_d) and qd frame reference currents (i_q^*, i_d^*):
  i_d presents a clear first-order dynamics because the reference i_d^* is directly computed with Q^* and the PI controller which stabilyses the real value to the reference value in the current loop imposes a firs-order dynamics. (Figure 4.20)
  i_q presents a strange dynamics which is more similar to a second-order dynamics. (Figure 4.21)

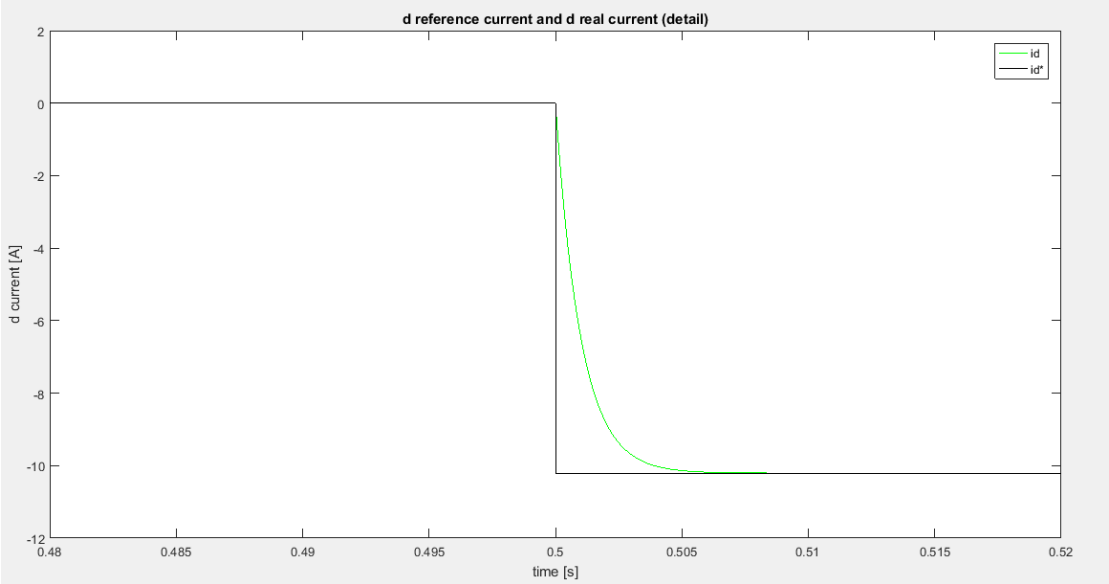

Fig. 4.20. dynamics of real and reference d currents (synchronous frame) (AC side of the VSC). Produced by the author with "Matlab/Simulink"

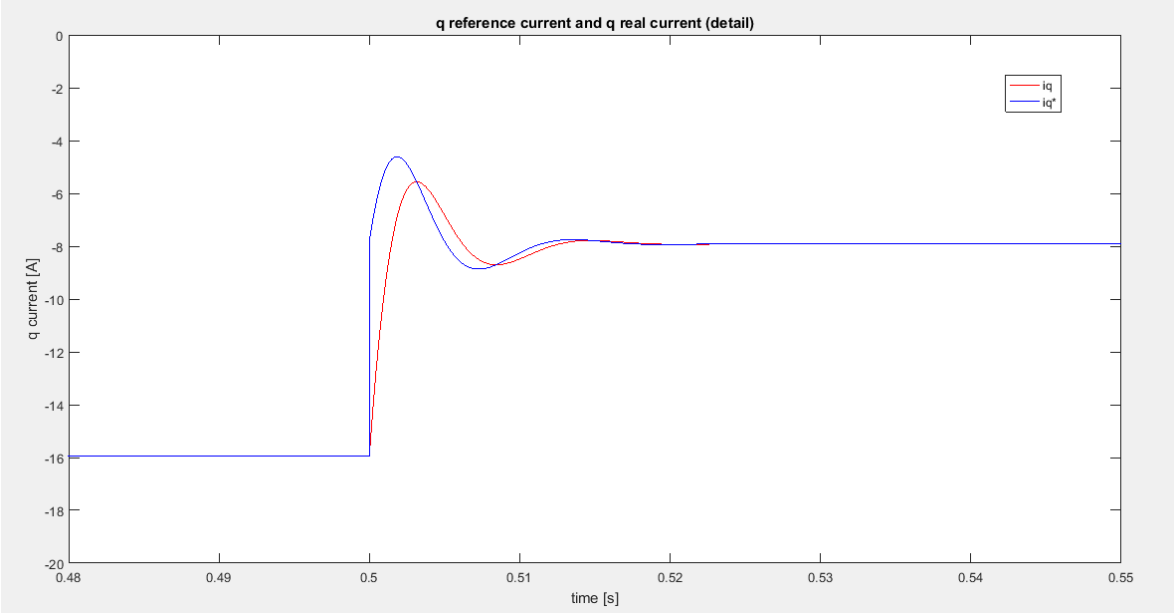

Fig. 4.21. dynamics of real and reference q currents (synchronous frame) (AC side of the VSC). Produced by the author with "Matlab/Simulink"

4.2.2. Solar Generation

All the components involved in the solar generation (PV Array, MPPT, DC/DC boost converter) has been modeled consulting the next academic articles:

''A Matlab/Simulink-Based Photovoltaic Array Model Employing SimPowerSystems Toolbox" by Samer Said, Ahmed Massoud, Mohieddine Benammar and Shehab Ahmed from the Department of Electrical Engineer, Qatar University [5]

"Modelado y Simulación de un Sistema Conjunto de Energía Solar y Eólica para Analizar su Dependencia a la Red Eléctrica" by M. Mikati, M. Santos and C. Armenta from Universidad Complutense de Madrid and Epsilon Embedded Systems (Gothenburg, Sweden) [6]

"Modelo Simulink en sfunction de un sistema fotovoltaico compuesto por un simulador de sol, panel y conversor" by Oscar Sánchez Rodríguez from UPC- Escola Tècnica Superior d'Enginyeria de Vilanova i la Geltrú [7]

The function of this model is to simulate a PV array by applying all the equations which describe its behavior. The only external outputs of this block are: the solar irradiance G, the temperature of the cells T_c, and the reference DC voltage in the DC bus $E_{DC}^{*} = 800V$. The model also simulates the effect of the Maximum Power Point Tracking algorithm in a very simplified way, and the DC/DC boost converter which injects power into the DC bus

PV array

- Electrical description of the solar cell:
  A solar cell can be described as a photo-generated current source, a diode and two resistances (one shunt resistance and one resistance in series) as illustrated in Figure 4.22:

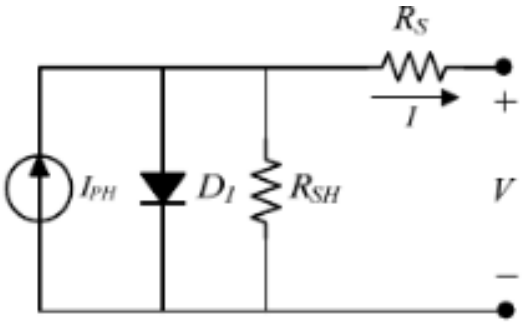

Fig. 4.22. equivalent circuit of a PV cell. Image extracted from "A Matlab/Simulink-Based Photovoltaic Array Model Employing SimPowerSystems Toolbox"[5]

Where I_{ph} is the photo-generated current, which depends on the irradiance and the temperature of the cell; R_s and R_{sh} are, respectively, the series and shunt resistances; I_d (which is not indicated in Figure 4.22) is the direct current in the diode; and I_{sh} are the losses in the parallel branch. I and V are the output current and voltage of the cell.

$$I = I_{ph} - I_d - I_{sh} \; (eq.23)$$

The equation for the photo-generated current is:

$$I_{ph} = \frac{G}{G_{ref}}\left[I_{sc} + K_{ti}\left(T_c - T_{c,ref}\right)\right] \; (eq.24)$$

Where $G_{ref} = 1000\ W/m^2$ is the reference irradiance (standard conditions), $T_{c,ref} = 25\ ºC$ is the reference cell temperature (standard conditions), I_{sc} is the short-circuit current at $T_{c,ref}$ and G_{ref} (provided by the manufacturer), and K_{ti} is the cell short-circuit current temperature coefficient (also provided by the manufacturer).

The equation for the direct current in the diode is:

$$I_d = I_o\left(exp\left[\frac{V + IR_s}{\eta V_t}\right] - 1\right) \; (eq.25)$$

$$V_t = \frac{\sigma T_c}{e} \; (eq.26)$$

$$I_o = I_{o,ref}\left(\frac{T_c}{T_{c,ref}}\right)^3 exp\left[eE_g\frac{\left(\frac{1}{T_{c,ref}} - \frac{1}{T_c}\right)}{\eta\sigma}\right] \; (eq.27)$$

$$I_{o,ref} = \frac{I_{sc}}{exp\left[\frac{V_{oc}}{N_s V_t}\right] - 1} \; (eq.28)$$

Where I_o is the reverse saturation current of the diode, $I_{o,ref}$ is the reference reverse saturation current (standard conditions), V_t is the equivalent voltage for temperature, $\sigma = 1.380648 \cdot 10^{-23}\ J/K$ is the Boltzmann constant, $e = 1.602176 \cdot 10^{-19}\ C$ is the charge of one electron, $\eta\ \epsilon[1,2]$ is the ideality factor of the diode (which models the mismatch of the real semiconductor material with the mathematical equations), E_g is the Gap Energy (or the minimum energy which has to be provided to a valence electron to excite it to the conduction band, a normal value for Silicon is $E_g = 1.12\ eV$), V_{oc} is the open-circuit voltage at $T_{c,ref}$ and G_{ref} (standard conditions) and it's provided by the manufacturer, N_s is the number of series

connected cells in a single PV module (the full array consists in series and parallel connected modules, as discussed further on), it's important to remark that it has been considered in the model that there are not parallel connected cells in a PV module, otherwise the equations would be slightly different.

The equation for the losses in the parallel branch is:

$$I_{sh} = \frac{V + IR_s}{R_{sh}} \ (eq. 29)$$

- <u>PV module subsystem</u>

  This model implements all the previous equations and generates the characteristic curves (V-I, P-I) of the PV module (Figure 4.23). It has six main blocks in it and one secondary block (comparator):

  - Photo Generated Current (Figure 4.24)
  - Voltage Temperature (Figure 4.25)
  - Reverse Current Reference (Figure 4.26)
  - Reverse Current Diode (Figure 4.27)
  - Direct Current Diode (Figure 4.28)
  - Losses in the parallel Branch (Figure 4.29)

  Notice that the voltage data points have been generated with a ramp signal (sweep) in order to generate the curves; the highest the slope of the voltage ramp is set, the quicker the program will compute and display the graphics. It's also important to remark that the system needs feedback in order to compute iteratively the curves.

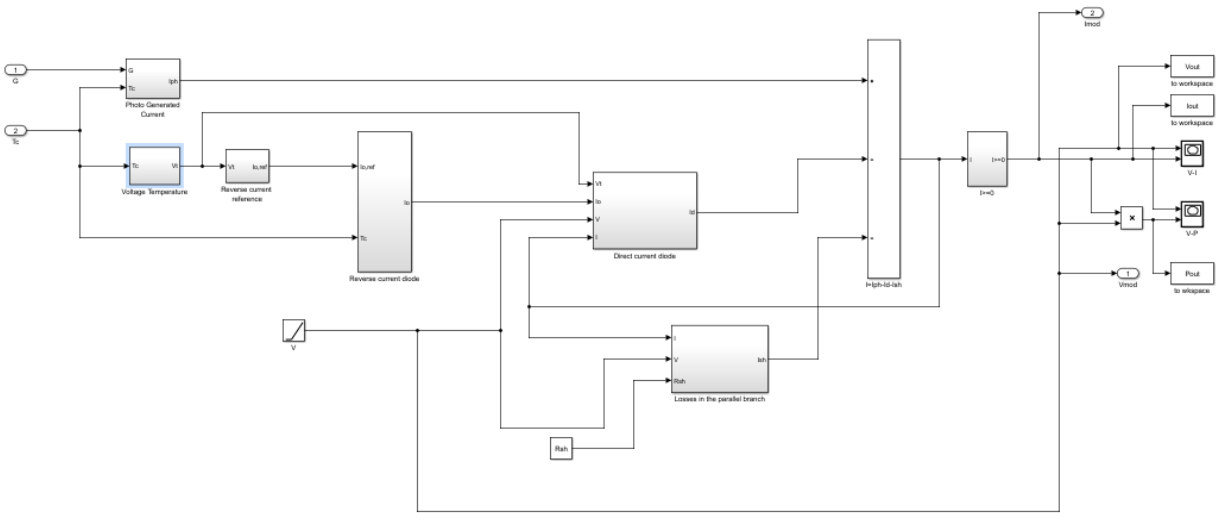

Fig. 4.23. Block implemented PV module system, following equation 23. Produced by the author with "Matlab/Simulink"

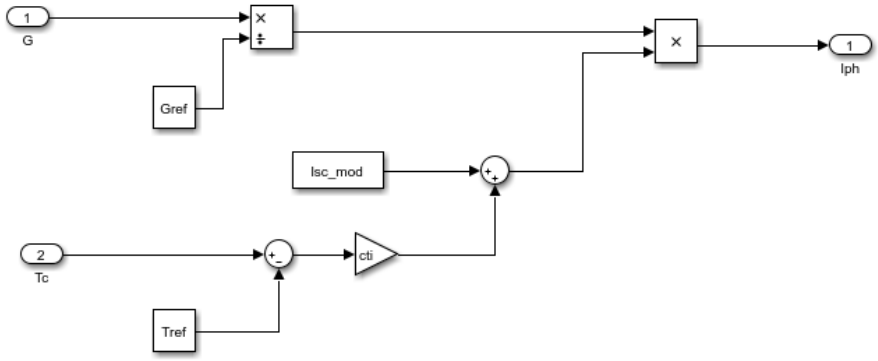

Fig. 4.24. Compute photo-generated current, following equation 24. Produced by the author with "Matlab/Simulink"

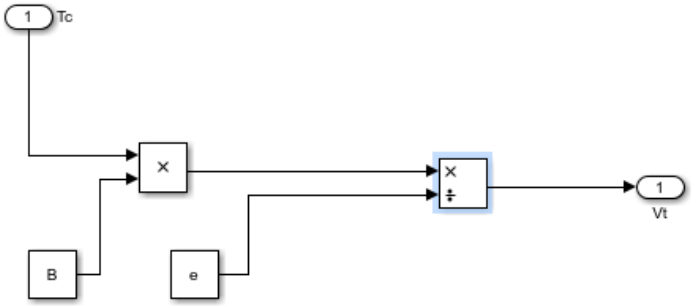

Fig. 4.25. Compute equivalent voltage for the temperature, following equation 26. Produced by the author with "Matlab/Simulink"

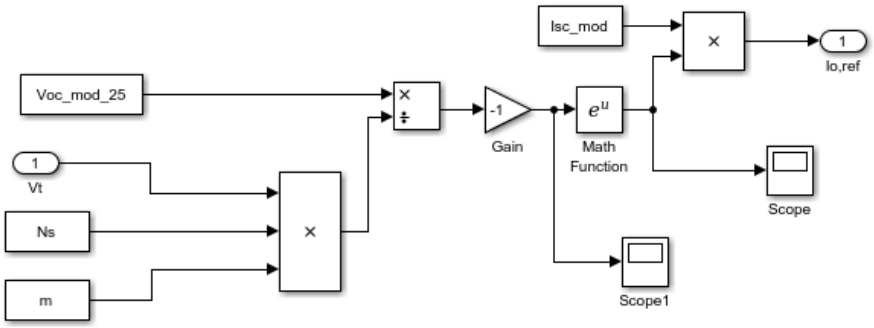

Fig. 4.26. Compute reference for the reverse saturation current of the diode, following equation 28. Produced by the author with "Matlab/Simulink"

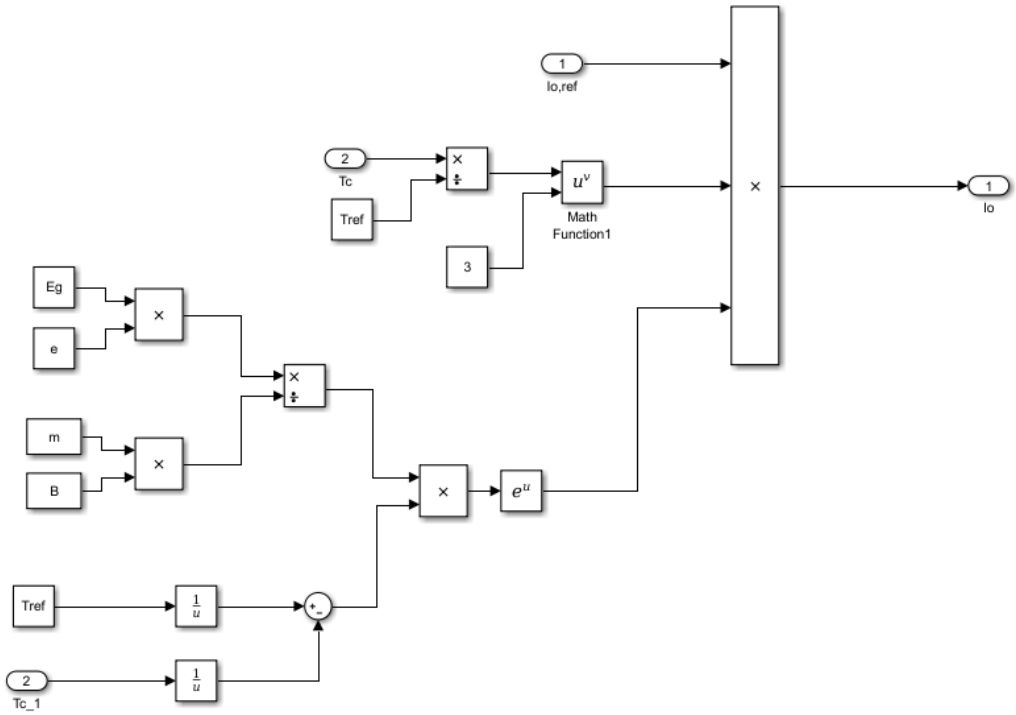

Fig. 4.27. Compute reverse saturation current of the diode, following equation 27. Produced by the author with "Matlab/Simulink"

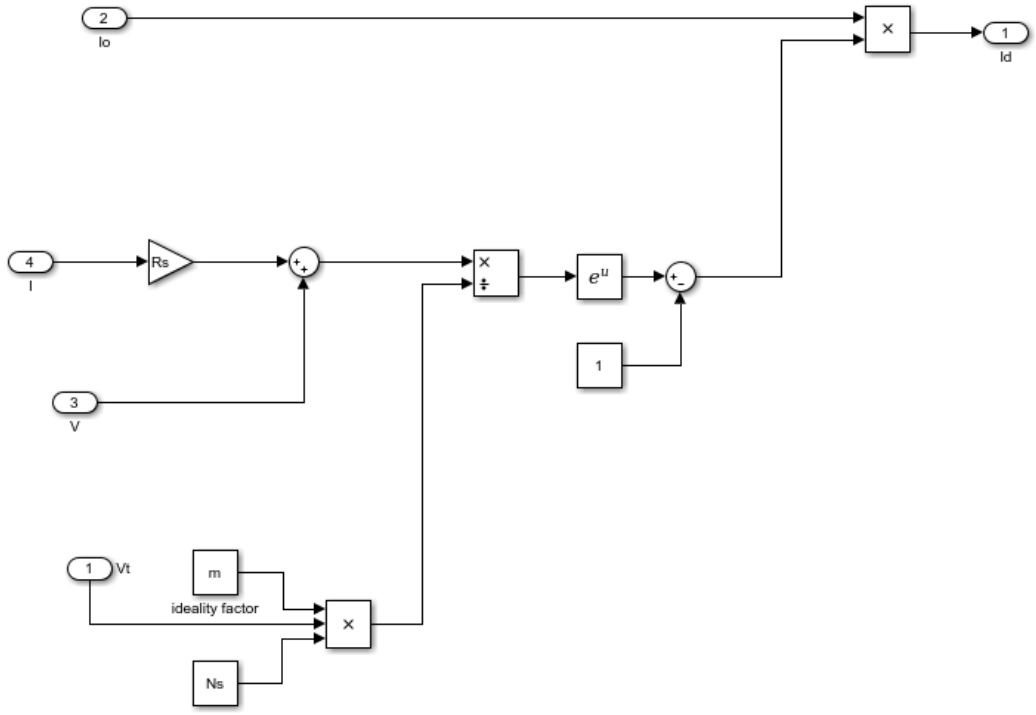

Fig. 4.28. Compute direct current of the diode, following equation 25. Produced by the author with "Matlab/Simulink"

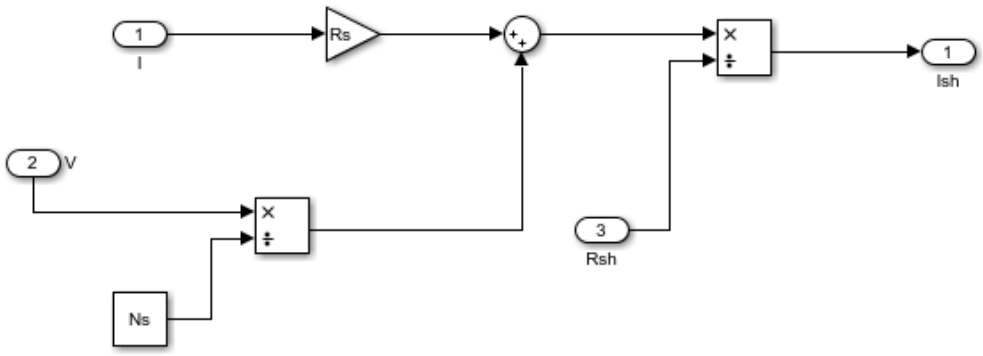

Fig. 4.29. Compute losses in the parallel branch, following equation 29. Produced by the author with "Matlab/Simulink"

- Results for a single PV module:

  Characteristic curves for a single PV module are shown in this section. The chosen PV panel is the polycrystalline Silicon 1STH-215-P manufactured by 1Soltech (can be found in a lot of specialized catalogues)

  PV module has the next characteristics:

Magnitude	**Value**
I_{sc} ($standard\ conditions$)	$7.84\ A$
V_{oc} ($standard\ conditions$)	$36.3\ V$
K_{ti} ($temp.\ \ coefficient\ for\ I_{sc}$)	$2.5 \cdot 10^{-2}\ A/K$
K_{tv} ($temp.\ \ coefficient\ for\ V_{oc}$)	$-0.0735\ V/K$
R_s	$0.3938\ \Omega$
R_{sh}	$313.3991\ \Omega$
N_s	$60\ cells\ in\ series$
$MPP\ (V_{mp}\ , I_{mp})\ (stand.cond.)$	$(\ 29\ V\ , 7.35\ A\ )$
$P_{mp}\ (stand.cond.)$	$213.15\ W$
$Area\ per\ module$	$1.57\ m^2$

Table. 4.1. Characterisitics of the Polychrystalline Silicon Panel 1Soltech 1STH-215-P. Provided from the manufacturer.

- Effect of solar irradiance:

  The maximum power that the PV module can give to the system is increasing with solar irradiance. For different values of irradiance (and same operating temperature 25ºC) different characteristic curves are obtained, as illustrated in Figure 4.30 and Figure 4.31.

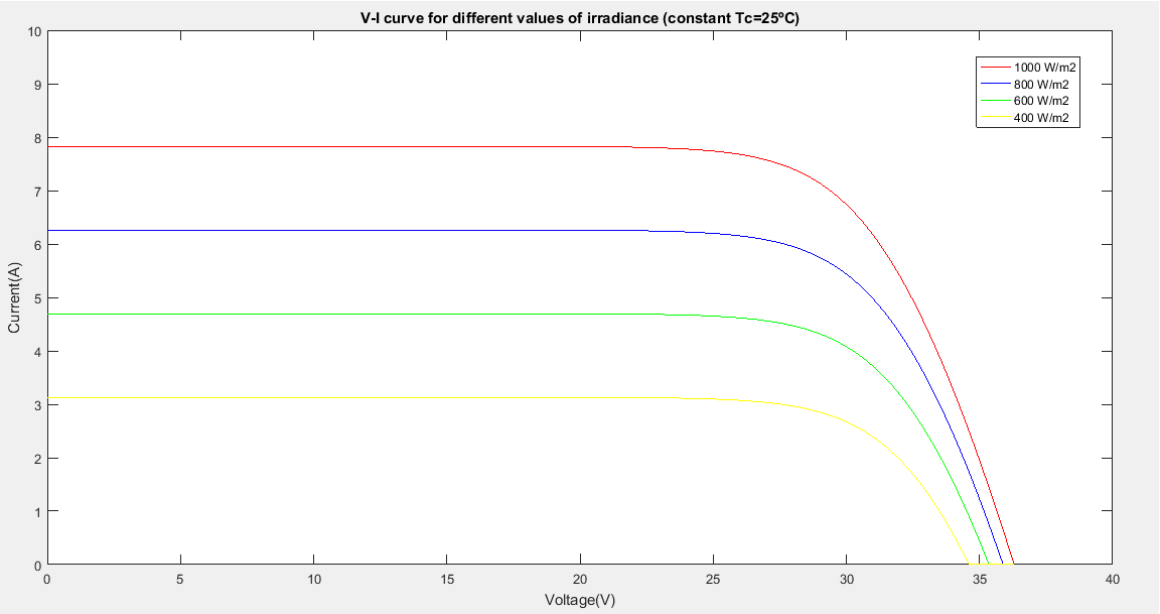

Fig. 4.30. Different V-I curves obtained for different values of irradiance. Produced by the author with "Matlab/Simulink"

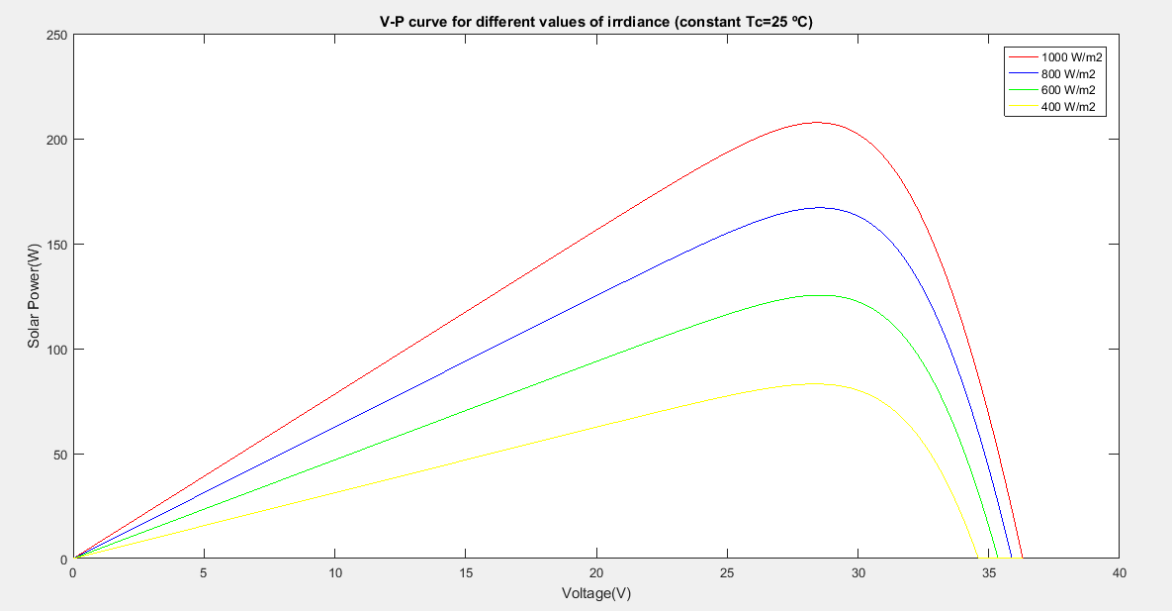

Fig. 4.31. Different V-P curves obtained for different values of irradiance. Produced by the author with "Matlab/Simulink"

- Effect of operating temperature:

  The maximum power that the PV module can give to the system is decreasing with the operating temperature. So the PV module is more efficient when working around 25ºC. For different values of temperature (and same irradiance 1000 W/m^2) different characteristic curves are obtained, as illustrated in Figure 4.32 and Figure 4.33.

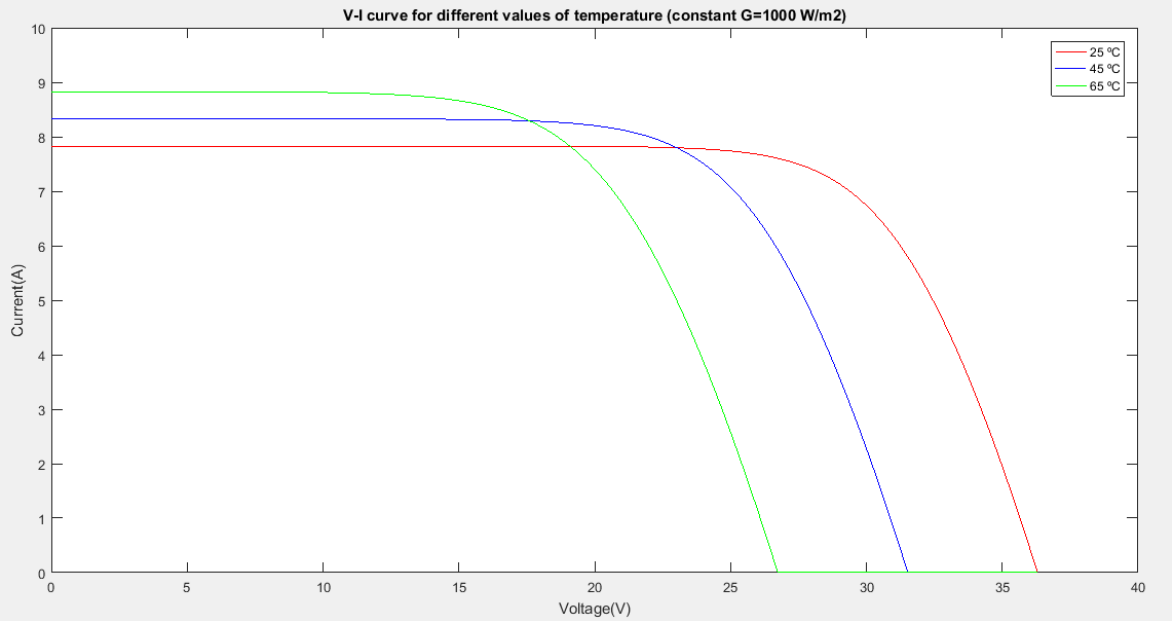

Fig. 4.32. Different V-I curves obtained for different values of temperature. Produced by the author with "Matlab/Simulink"

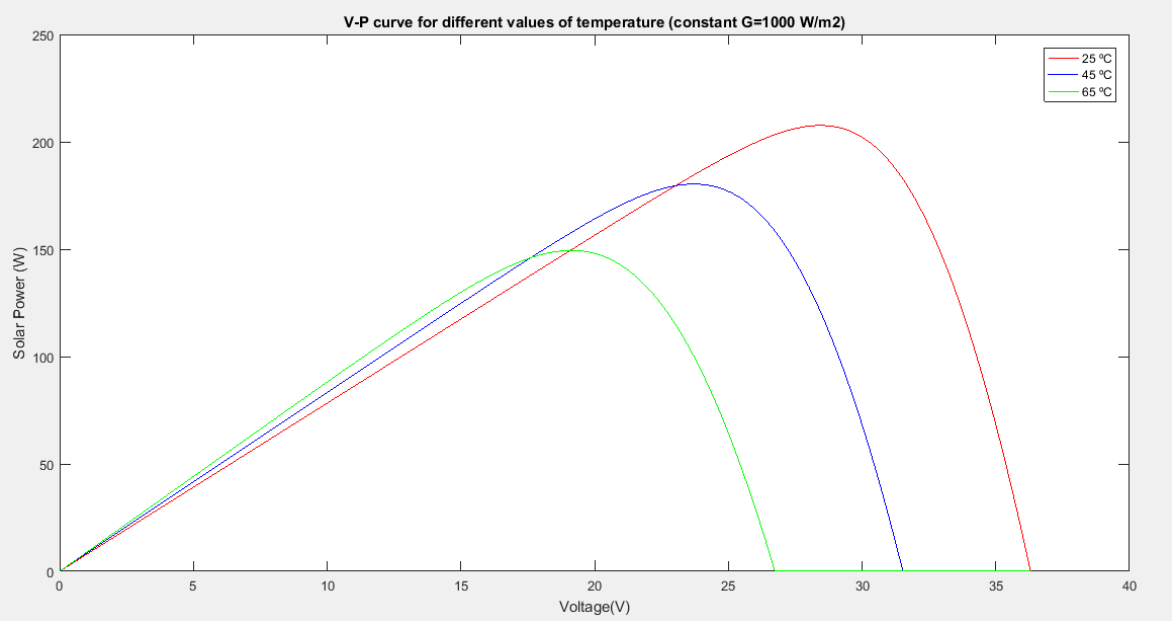

Fig. 4.33. Different V-P curves obtained for different values of temperature. Produced by the author with "Matlab/Simulink"

- Standard Conditions: real values vs. simulated values

  It can be observed in Table 4.2 that the error between the real values and the simulated values is not significant, so the proposed model works properly. This error must be caused by the indeterminacy of some parameters like the ideality factor $\eta = 1.2$ or the energy gap $E_g = 1.12\ eV$, which are tabulated values different to the real ones.

Magnitude	Real Value	Simulated Value	Relative Error
I_{sc}	$7.84\ A$	$7.83\ A$	0.13 %
V_{oc}	$36.3\ V$	$36.26\ V$	0.11 %
V_{mp}	$29\ V$	$28.8\ V$	0.69 %
I_{mp}	$7.35\ A$	$7.29\ A$	0.82 %
P_{mp}	$213.15\ W$	$209.66\ W$	1.63 %

Table. 4.2. Comparison between the real PV module and the simulated PV module

- Electrical description of the PV Array:

  The PV Array is a series-parallel association of individual modules (which are also a series association of individual cells)

  This association creates a solar generation which depends on the PV module used (assuming that all the modules are the same), on the parallel-series connected modules, on the irradiance and on the temperature of operation.

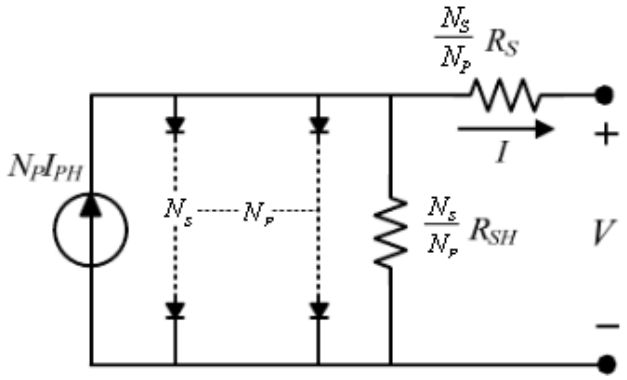

Fig. 4.34. equivalent circuit of a PV Array. Image extracted from "A Matlab/Simulink-Based Photovoltaic Array Model Employing SimPowerSystems Toolbox"[5]

The behavior of the full array is described by equation 30:

$$I = m_p I_{ph} - m_p I_o \left(exp\left[\frac{\frac{V}{m_s} + \frac{IR_s}{m_p}}{\eta V_t} \right] - 1 \right) - \frac{\left(\frac{m_p}{m_s} V + IR_s \right)}{R_{sh}} \quad (eq.30)$$

Where $(m_p\ , m_s)$ are, respectively, the parallel connected modules and the series connected modules in the array.

- PV Array subsystem:

  The PV Array subsystem is a very simple block which has as input the V-I curve of the single module and the number of parallel-series association, and produces (output the V-I and P-I curves of the full array).

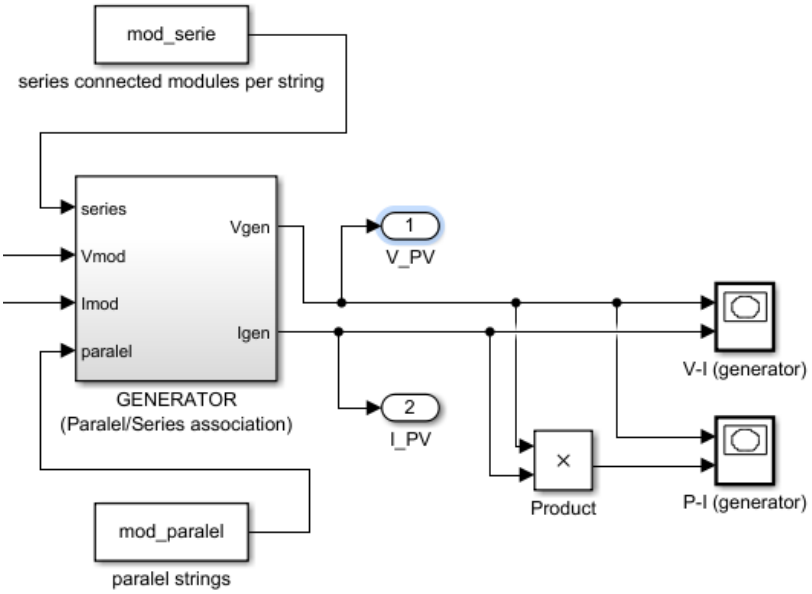

Fig. 4.35. Compute PV Array Charactisristic Curves, following equation 30. Produced by the author with "Matlab/Simulink"

- PV Array Results:
  - Standard Conditions: Simulated Values

    Characteristic curves of the PV array are displayed in Figure 4.36 and Figure 4.37 for $G = 1000\ W/m^2$ and $T_c = 25\ ºC$.

    Model of the PV module: polycrystalline Silicon 1STH-215-P manufactured by 1Soltech (with the same module parameters as displayed in Table 4.3)

    Array Characteristics: $m_p = 20\ modules$, $m_s = 5\ modules$

    Total Area of the Array: 157 m^2

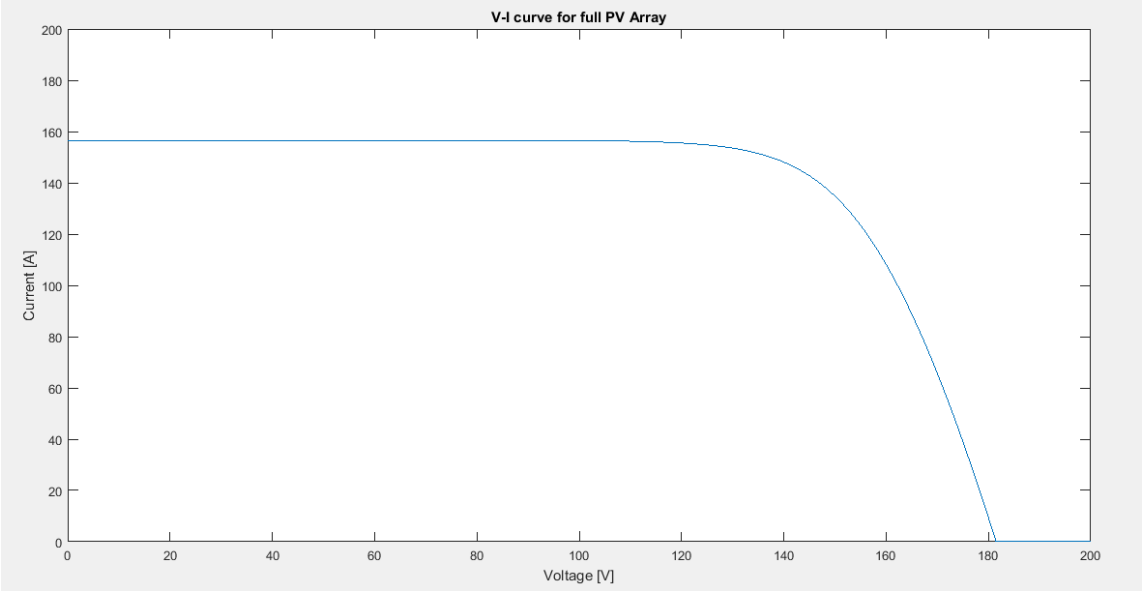

Fig. 4.36. V-I curves obtained for full PV Array. Produced by the author with "Matlab/Simulink"

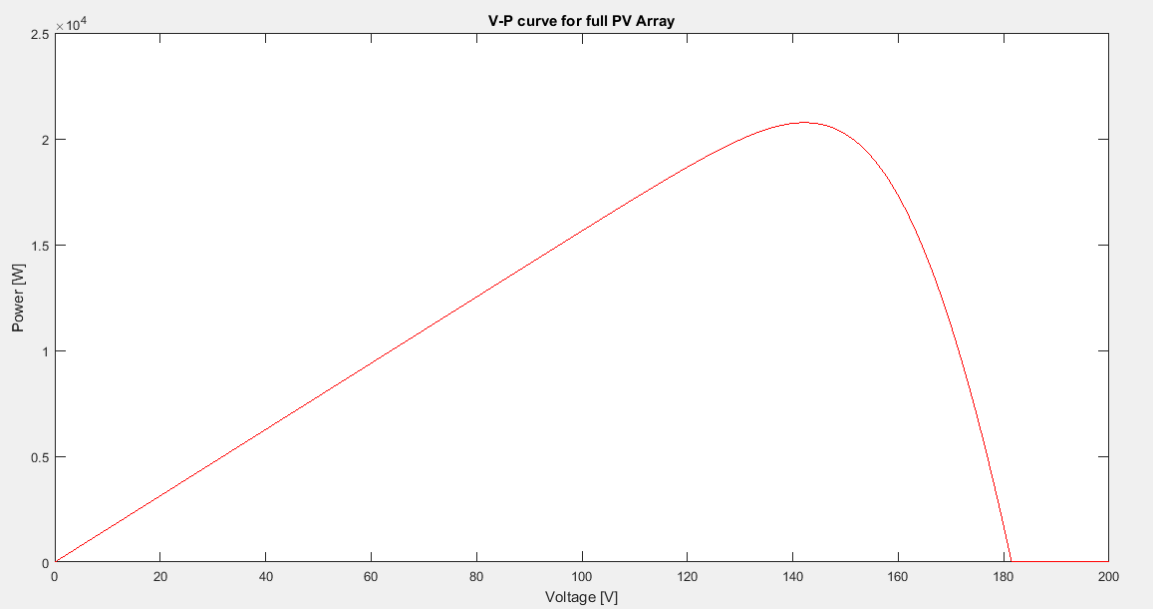

Fig. 4.37. V-I curves obtained for full PV Array. Produced by the author with "Matlab/Simulink"

- Standard conditions: obtained values for full array

Magnitude	Real Value
I_{sc}	$156.6\ A$
V_{oc}	$191.5\ V$
V_{mp}	$142.5\ V$
I_{mp}	$145.7\ A$
P_{mp}	$20.76\ kW$

Table. 4.3. Simulated values for full PV Array of 20 parallel connected modules and 5 series connected modules. Notice that this system is capable of producing 20.76 kW in 157 m^2 of occupied space.

MPPT and DC/DC converter

- Maximum Power Point Tracking Algorithm:

  The maximum power point tracking is a technique used with photovoltaic arrays to maximize the power extraction regardless of the irradiance and temperature conditions.

  In this case, the MPPT algorithm tracks the maximum power point (V_{mp}, I_{mp}) and injects the maximum power to the DC bus through a DC/DC boost converter which converts the voltage from $V_{mp}(G, T_c)$ to $E_{DC}^{*} = 800\ V$ (reference voltage in the DC bus controlled by the VSC converter).

  The MPPT algorithm computes the required duty cycle (D) for the boost converter in order to guarantee maximum power. There are four main different MPPT algorithms:

  - Perturbe and Observe (Hill-Climbing)
  - Incremental Conductance
  - Current Sweep
  - Constant Voltage* *for some authors, this is not a MPPT technique in strict sense

  The most used and simplest of these four algorithms is the first one. The P&O algorithm is a very intuitive way of tracking the MPP as is explained in the diagram of Figure 4.38.

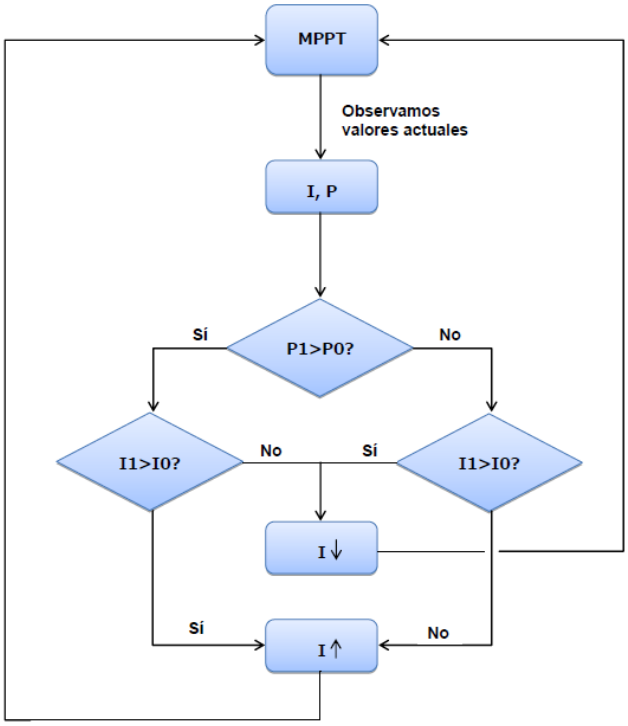

Fig. 4.38. Diagram explaining MPPT algorithm. Image extracted from "Modelo Simulink en sfunction de un sistema fotovoltaico compuesto por un simulador de sol, panel y conversor"[7]

This algorithm compares the produced power in the instant (t) with the produced power in the previous instant $(t - \Delta t)$ and changes the duty cycle of the converter in order to increase/decrease the value of the current I_{PV} as needed (Some MPPT algorithms change the value of the voltage V_{PV} instead of the current, as seen in Figure 4.39). The power supplied by the PV Array after the MPPT is always oscillating around the maximum power (Hill-Climbing concept).

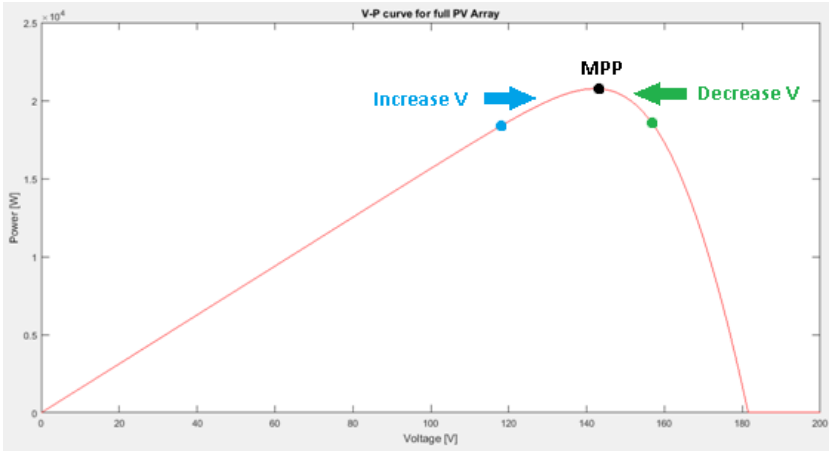

Fig. 4.39. Hill Climbing concept in a V controlled P&O MPPT algorithm

Following the first algorithm (current controlled P&O MPPT), four possible cases (states) can be easily analyzed, which are resumed in Table 4.4 and Figure 4.40, taking into account the next equation:

$$D = \frac{t_{ON}}{T_c} \ (eq. 31)$$

Where $t_{ON}\ [s]$ is the time when the transistor is ON (ohmic region in MOSFETs and saturation region in BJTs) in a period of commutation. $T_c\ [s]$ is the commutation period.

state	$I_{PV}(t)$	$P_{PV}(t)$	$t_{ON}(t)$	$D(t)$	$I_{PV}(t+\Delta t)$
1	$< I_{PV}(t-\Delta t)$	$< P_{PV}(t-\Delta t)$	increase	increase	$> I_{PV}(t)$
2	$< I_{PV}(t-\Delta t)$	$> P_{PV}(t-\Delta t)$	decrease	decrease	$< I_{PV}(t)$
3	$> I_{PV}(t-\Delta t)$	$< P_{PV}(t-\Delta t)$	decrease	decrease	$< I_{PV}(t)$
4	$> I_{PV}(t-\Delta t)$	$> P_{PV}(t-\Delta t)$	increase	increase	$> I_{PV}(t)$

Table. 4.4. States of the MPPT algorithm.

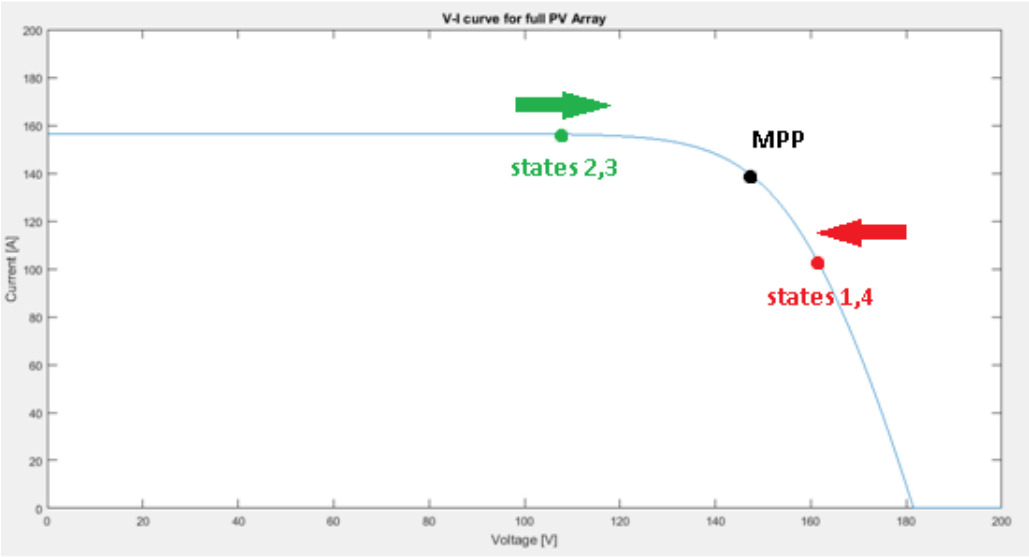

Fig. 4.40. Response to the states of the MPPT algorithm. In states 1 and 4, current will increase in order to track the MPP; in states 2 and 3, current will decrease.

- DC/DC Boost converter electrical description:

  The boost DC/DC converter is a power electronics converter which gives a higher output DC voltage from a lower input DC voltage. Their components are: an inductance in series with the input voltage source, a switch in a parallel branch, a diode in series with the inductance, and a capacitor in a parallel branch (Figure 4.41). In this case, the switch (transistor in commutation) is controlled with a PWM technique which can be described by the duty cycle (D). The duty cycle is computed by the MPPT every Δt (as described previously).

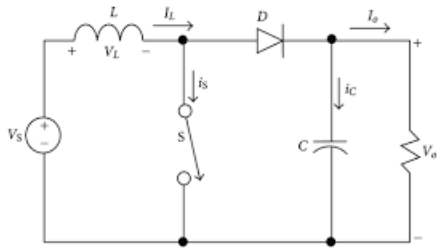

Fig. 4.41. DC/DC Boost converter. Image extracted from "Electrònica. Grau en Enginyeria de Tecnologies Industrials, ETSEIB – Emili Lupon"[8]

- MPPT + DC/DC Boost converter subsystem:

  The Simulink model of the MPPT and the DC/DC Boost converter has been extremely simplified due to two principal reasons:

  - Simplicity. The model proposed is not realistic in the practical way (the real system will not work like the simulation model, commutation is not modeled, power is not oscillating around the MPP, injected power to the DC bus is constant and equal to the maximum power for that climate conditions)
  - Simulation Speed: Simulink takes hours to simulate a few seconds of the realistic model but can simulate this model very fast (less than a minute)

  The MPPT is substituted for a $\max(P_{PV})$ function which injects the maximum power to the average DC/DC converter which injects this power into the bus at $E_{DC}^{*} = 800\,V$. Figure 4.42 and Figure 4.43

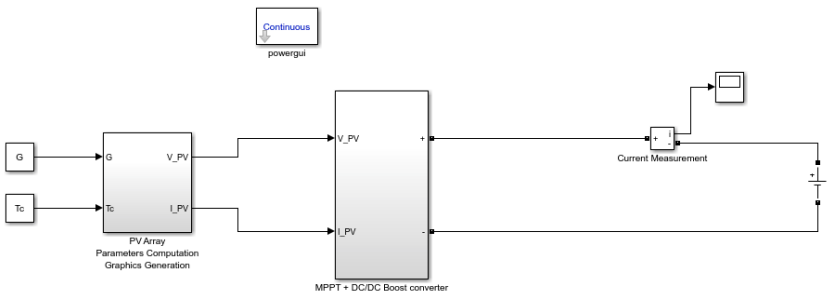

Fig. 4.42. Complete Solar Generation System, with PV array (left) and MPPT+DC/DC (right). Produced by the author with "Matlab/Simulink"

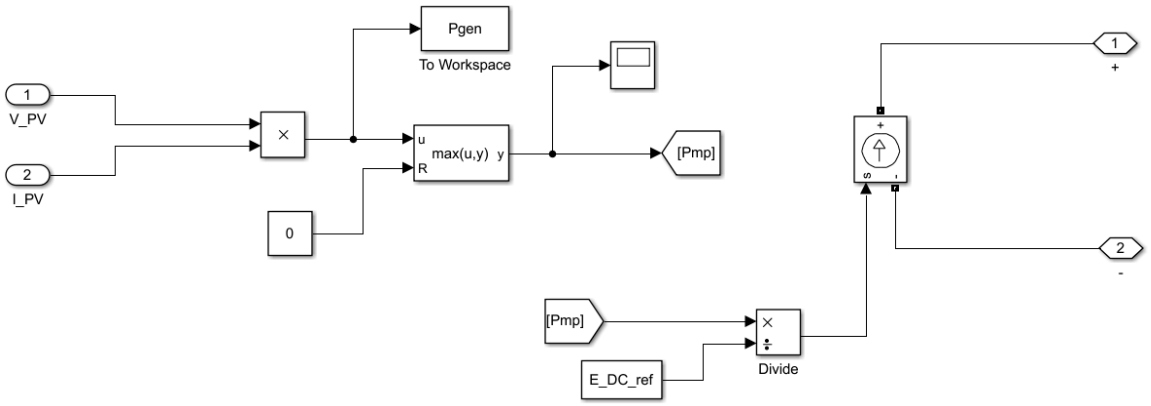

Fig. 4.43. simplified MPPT (left) and average DC/DC (right). Produced by the author with "Matlab/Simulink.

Particularities of the model:

- The speed for this system to reach the MPP is determined by the slope of the voltage ramp in the PV module block. The highest the slope of the ramp is, the quickest the system will reack the MPP
- For an unknown reason, when the slope of the voltage ramp is too high, the model injects a power lower than the maximum ($aprox.\ \ P_{PV} \cong 0.95 P_{mp}$). It´s important to choose a suitable slope in order to get the maximum power in short time period.
- The controllable current source is complying equation 32:

$$I_{DC} = \frac{P_{DC}}{E^*_{DC}} \cong \frac{P_{mp}}{800\ V}\ (eq.32)$$

- PV Array + MPPT + DC/DC boost converter results:

Figure 4.44 and Figure 4.45 show, respectively, the power injected to the DC bus and the current in the DC bus. It can be observed that the system takes some time to reach the maximum power. When the power gets its maximum, the value of the DC current stabilizes. Table 4.5 shows some relevant numerical results.

P_{mp}	$20.76\ kW$
$P_{DC}\ (stable\ value)$	$20.76\ kW$
$relative\ error: \left[(P_{mp} - P_{DC)}/P_{mp}\right] \cdot 100$	0%
$t_P\ (time\ to\ reach\ P_{DC})$	$0.308\ s$
$t_s\ (time\ of\ the\ simulation)$	$1.1s$
$slope\ of\ the\ voltage\ ramp$	$100\ V/s$
$I_{DC}\ (stable\ value)$	$25.95\ A$

Table. 4.5. Results of the simulation.

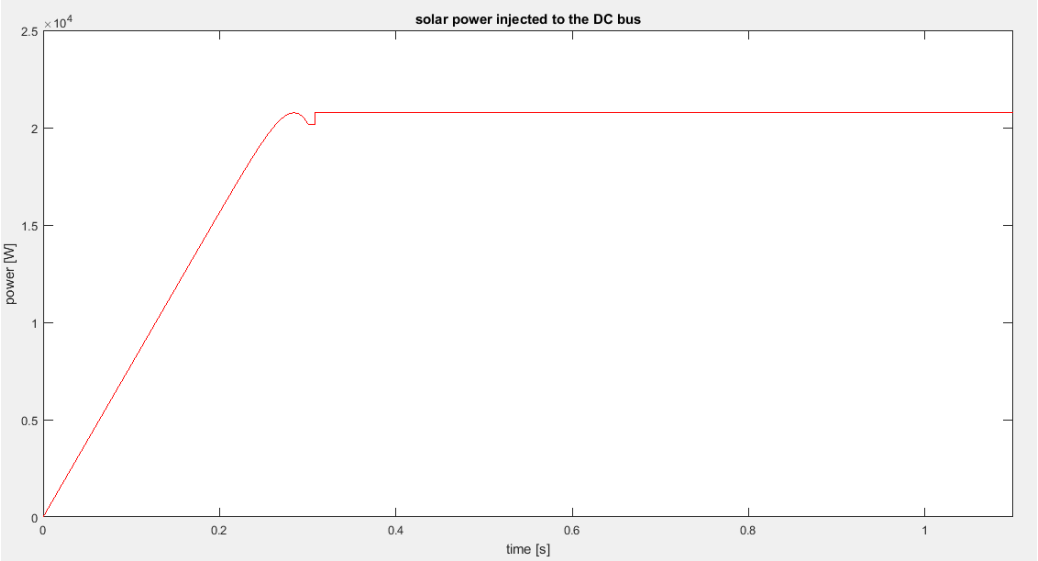

Fig. 4.44. Solar power injected to the DC bus. Produced by the author with "Matlab/Simulink"

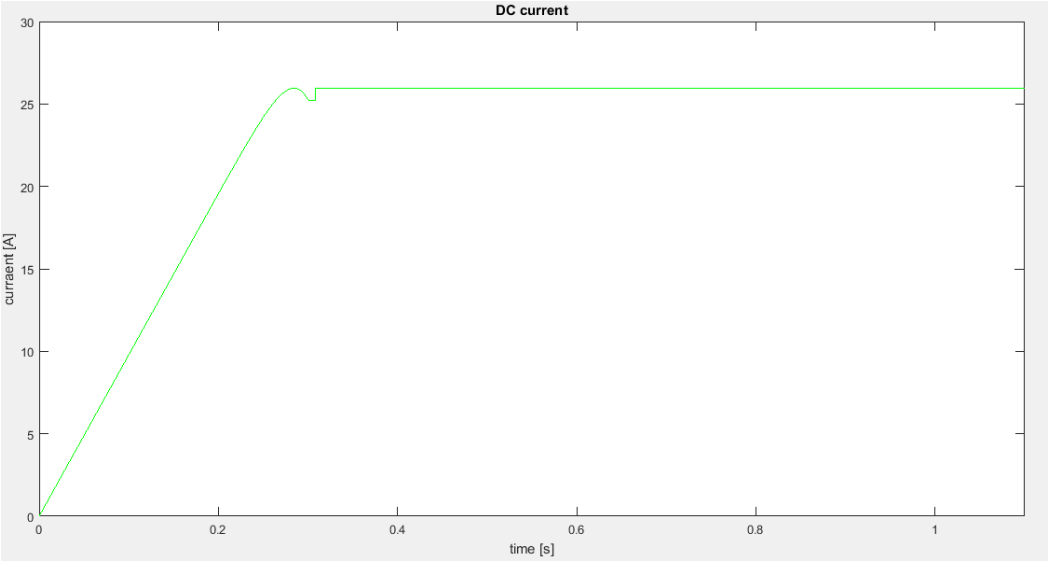

Fig. 4.45. Current in the DC bus due to solar power injection. Produced by the author with "Matlab/Simulink"

4.2.3. Storage System

All the components of this model have been modeled using the own knowledge of the author about power electronics and storage systems, oral sources (mainly professor and co-director of the project Eduard Prieto), *Mathworks* official forum [10.] and "Topology of a Bidirectional Converter for Energy Interaction between Electric Vehicles and the Grid – Jiuchun Jiang, Yan Bao, Le Yi Wang – School of electrical engineering of Beijing" [9]

The function of this model is to simulate how the storage system of the microgrid works. It contains two main components: the battery and the bidirectional DC/DC converter which charge and discharge the battery at the required voltages.

Battery

The battery is an essential part of the microgrid because it´s used to store the energy which is not used in certain moments of operation (When the demanded power is lower than the generated power). This energy can be supplied to the system when the demand has a peak and the PV solar generation is not enough to cover it.

Batteries are complex electrochemical elements and their mathematical modeling is completely out of the scope of this project. For this simulation the Simulink preset model of a battery (Figure 4.46) is used because of these reasons:

- Reliability. Mathworks is a very reliable source.
- Flexibility. Different types of batteries can be chosen (materials, capacities, other parameters)
- Time. Modeling a battery from the beginning would be too time consuming.

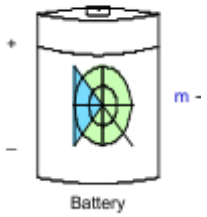

Fig. 4.46. Preset model of a generic battery "Matlab/Simulink"

- Capacity of a battery and State of Charge:

  The rated capacity of the battery is its energy capacity under nominal conditions and it's provided by the manufacturer. There is a very wide range of batteries with different capacities. This magnitude is given in $[Ah]$, which relates the time that the battery can provide a determined value of current (for example, if the battery has a rated capacity of 10Ah and it's fully charged, it can provide 10 Amperes of current during 1 hour, 5 Amperes during two hours, etc.).

  The State of charge is the level of available energy in the battery in relation with its capacity. It's very important to take into account when sizing the batteries that its state of charge has to be into a certain range, so it can't be very high neither very low (normally between 5 and 90%).

- Chosen parameters of the battery for the simulation:

  The parameters for the battery chosen in this simulation are not the real ones (the battery in the microgrid is not like this one). But some of these values have been chosen in order to show clear results. Table 4.6.

Parameter	Value [unit]	Real/Unreal
Type	$Lithium - Ion$	Real
Nominal Voltage	$200\ V$	Real
Rated Capacity	$4\ Ah$	Unreal (too low for the benefit of the simulation)
Initial SOC	$50\ \%$	Real
Fully charge voltage	$232.8\ V$	Real

Table. 4.6. Parameters of the battery

DC/DC converter

- Electrical/ Electronical description of the converter:

  This converter has two main functions:

  - Inject power from the DC bus (800V) to the battery (around 200V) → Buck
  - Inject power from the battery (around 200V) to the DC bus (800V) →Boost

  The required converter in this case is a bidirectional Buck-Boost converter, which is showed in Figure 4.47.

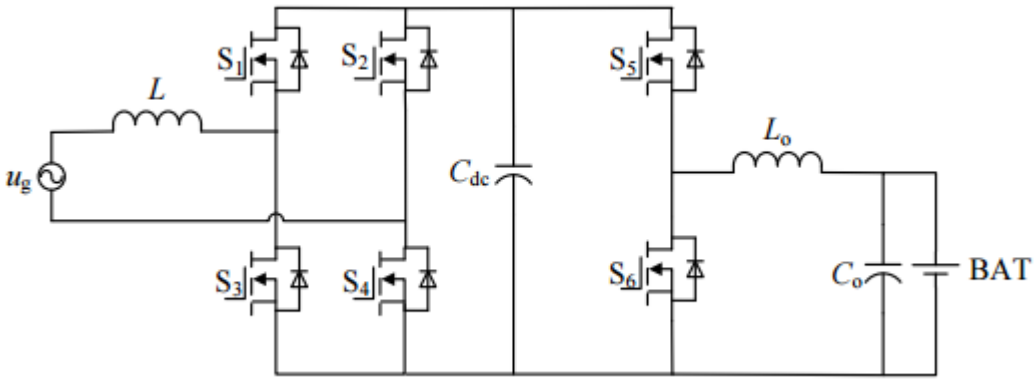

Fig. 4.47. Non-isolated On-board Bidirectional DC/DC Buck-Boost converter. Image extracted from "Topology of a Bidirectional Converter for Energy Interaction between Electric Vehicles and the Grid"[9]

- Description of the average model:

  The simulation of this converter doesn't take into account the commutation of the transistor (neither the commutation losses), so the model only works with average voltages, currents and power. The model consists in two main subsystems: power subsystem and control subsystem (Figure 4.48).

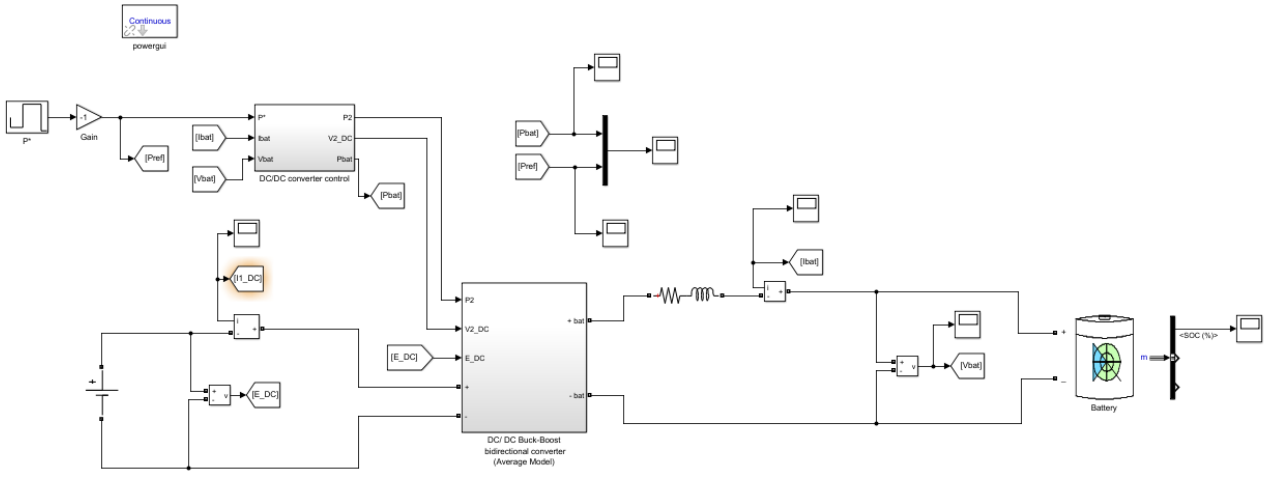

Fig. 4.48. Average model for the bidirectional converter. The central block is the Power subsystem and the block on the top is the Control subsystem. Produced by the author with "Matlab/Simulink"

- Description of the power subsystem:

  This subsystem consists in one controllable voltage source connected to the battery (with a RL branch connected in series) and one current controllable source connected to the DC bus. (Figure 4.49).

  The current source gives the necessary current in order to transfer the provided power from the battery to the DC bus (can be positive or negative) at the reference DC voltage $E_{DC}^{*} = 800V$, following next equation 33

$$I_{DC} = \frac{P}{E_{DC}^{*}} \ (eq.33)$$

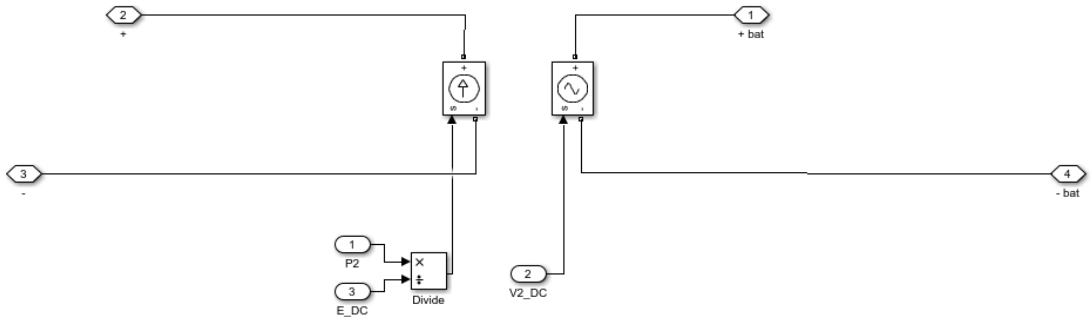

Fig. 4.49. Power subsystem. Produced by the author with "Matlab/Simulink"

- Description of the control subsystem:

  The control subsystem consists in two main blocks:

  - Reference Computation
  - Control Loop

  The reference computation block computes the required current (I_{BAT}^{*}) with equation 34

$$I_{BAT}^{*} = \frac{P^{*}}{V_{BAT}} \ (eq.34)$$

  The control loop stabilizes the real current (I_{BAT}) to the previously computed current reference with a PI controller.

  The equation which describes the electrical behavior in the battery side is:

$$V(t) - V_{BAT}(t) = RI_{BAT}(t) + L\frac{d}{dt}I_{BAT}(t) \ (eq.35)$$

  Being V the voltage of the controllable voltage source of the converter.

The Lagrange transformation of this equation is:

$$V(s) - V_{BAT}(s) = (R + Ls)I_{BAT}(s)\ (eq.36)$$

This equation can be decoupled as follows: (Figure 4.50):

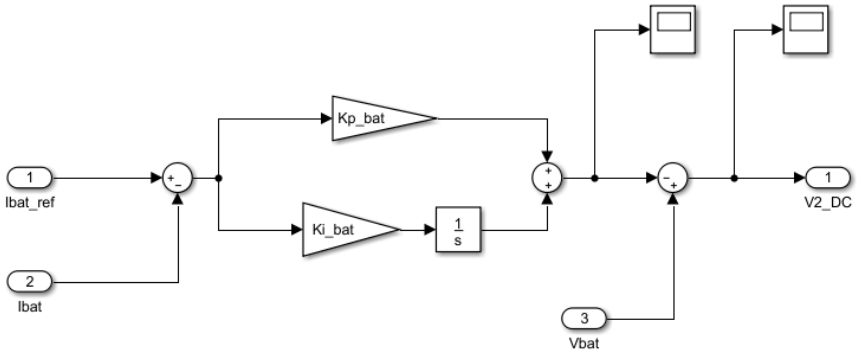

Fig. 4.50. PI controller for the Battery current. Produced by the author with "Matlab/Simulink".

The equations for the PI controller are:

$$PI(s) = K_{p\_BAT} + \frac{K_{i\_BAT}}{s}\ (eq.37)$$

$$K_{P\_BAT} = {}^{L_{BAT}}/_{\tau_{BAT}}\ (eq.38)$$

$$K_{i\_BAT} = {}^{R_{BAT}}/_{\tau_{BAT}}\ (eq.39)$$

The proposed values for the simulation are: $\boldsymbol{R_{BAT} = 0.1\ \Omega}$, $\boldsymbol{L_{BAT} = 10^{-3}H = 1\ mH}$, $\boldsymbol{\tau_{BAT} = 10\ ms}$.

- Results of the simulation:

  The next two figures (Figures 4.51 and 4.52) represent, respectively, the power first-order dynamics and the State of charge of the battery. When the battery is injecting power to the DC bus the state of charge decreases. When the solar generation is higher than the demand, that excess can be injected to the battery, increasing its state of charge.

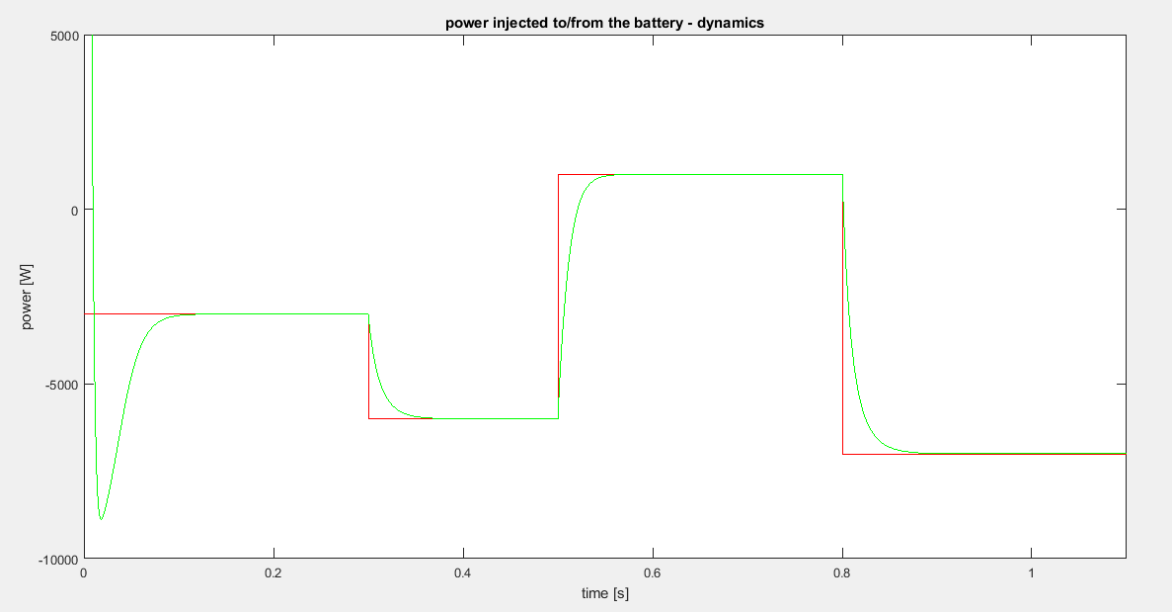

Fig. 4.51. Battery power dynamics. Produced by the author with "Matlab/Simulink"

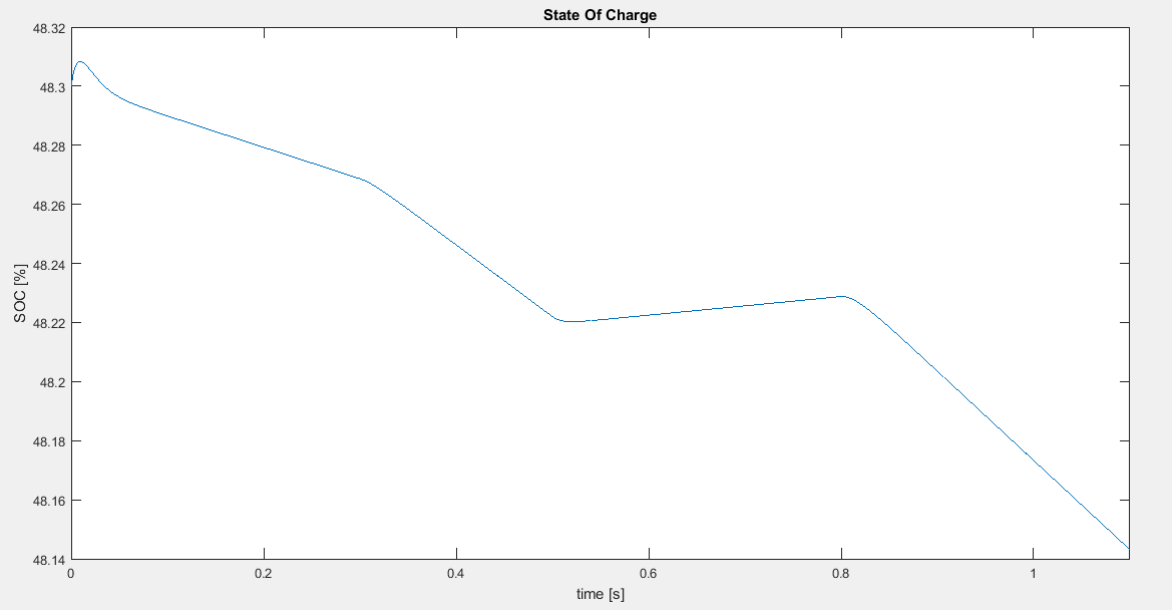

Fig. 4.52. State of charge. Produced by the author with "Matlab/Simulink"

Notice that when the power reference is positive, the state of charge increases (DC bus supplying power to the battery, from t=0.5 s to t=0.8 s). When the power reference is negative, the state of charge of the battery decreases (Battery injecting power to the DC bus). It can be observed the bidirectional behavior of the system and the need of using a Buck-Boost converter.

4.2.4. High level control system

- Active power reference for the battery:

  Let's define ΔP as the difference between the solar generated power and the demanded power, equation 40:

  $$\Delta P = P_{solar} - P_{demand} \ (eq. 40)$$

  Then, three different states can be defined:

  - $\Delta P < 0$

    The active power demanded is higher than power generated by the PV panels, so the battery must inject power to the DC bus, decreasing its SOC.
  - $\Delta P = 0$

    Battery is neither being charged nor discharged
  - $\Delta P > 0$

    The solar generation is higher than the active power demanded so the power surplus is charged to the battery

  But the SOC of the battery has to be between a security interval in order to ensure good functioning: $SOC \ \epsilon \ [5\%, 90\%]$, so 9 different states can be defined, as shown in Table X:

	$\Delta P < 0$	$\Delta P = 0$	$\Delta P > 0$
$SOC \leq 5\%$	WARNING: additional power source needed (Diesel Generator)	Nothing	DC bus injects $\lvert\Delta P\rvert \ [W]$ to the battery (charge
$5\% < SOC < 90\%$	Battery injects $\lvert\Delta P\rvert \ [W]$ to the DC bus (discharge)	Nothing	DC bus injects $\lvert\Delta P\rvert \ [W]$ to the battery (charge)
$SOC \geq 90\%$	Battery injects $\lvert\Delta P\rvert \ [W]$ to the DC bus (discharge)	Nothing	WARNING: non-profitable power (Sink DC load)

Table. 4.7. Different States for the active power reference of the battery

- Reactive power reference for the VSC controller:

  This reference has been set to zero for simplicity purposes $Q^* = 0 \ var$

- Zero Net-Metering Control:

  Using PI controller:

$$I^*_{grid} = 0\ A$$

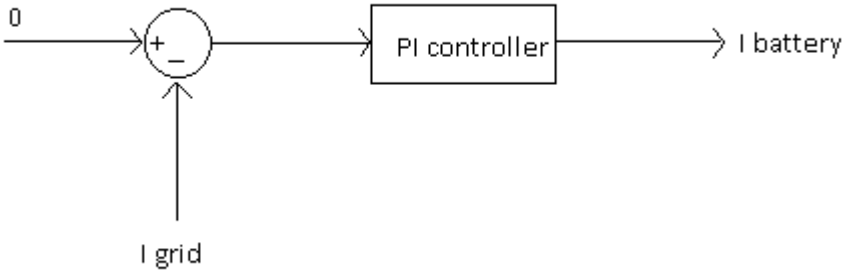

Fig. 4.53. PI controller for achieving Zero Net-Metering.

4.2.5. Loads and other components

- Three- phase loads

  All the AC loads have been modeled as three-phase loads because single-phase loads are connected to one of the phases and to the neutral phase (N), which is a four wire that has not been modeled in any of the previous components. The demand has been grouped in a dynamic AC three-phase load as shown in Figure X.

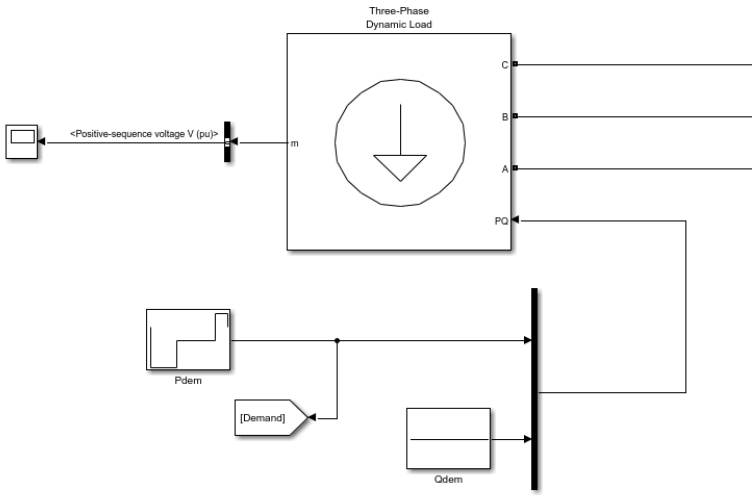

Fig. 4.54. Demand grouped in a three-phase PQ dynamic load. Produced by the author with "Matlab/Simulink"

- DC loads

  There can be two main types of DC loads in the system:

  - DC engines

- Sink DC load: This type of load is only connected to the system when $\Delta P > 0$ and $SOC \geq 90\%$. It consists in a Joule effect sink which consumes the non-profitable generated solar power.

- Electric Vehicle Charger

  EV Chargers can be easily integrated in the system. They can be modeled as batteries and connected to the DC bus with a DC/DC buck (unidirectional) converter (Figure 4.55). The converter is necessary because the batteries must be charged at 12-15V approximately, and the voltage of the DC bus is 800V.

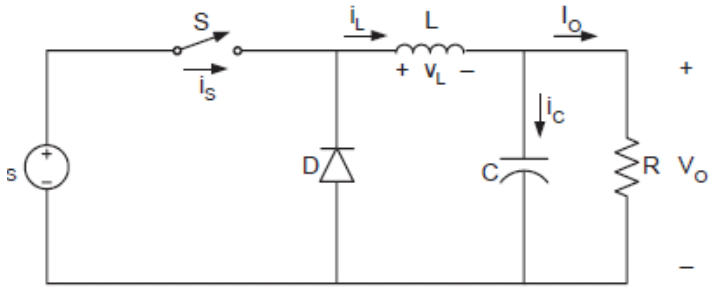

Fig. 4.55. DC/DC Boost converter. Image extracted from "Electrònica. Grau en Enginyeria de Tecnologies Industrials, ETSEIB – Emili Lupon"[8]

- Diesel Generator

  Additional non-renewable power source which is only connected to the system when $\Delta P < 0$ and $SOC \leq 5\%$ in order to cover the electrical demand when solar generation is not enough and batteries are empty. This type of generators generate AC current so they must be connected directly to the AC loads (not to the DC Bus)

5. Conclusion

After running the most important simulations of the designed system and displaying the most relevant results in the main body of this report, we can extract some important conclusions.

In order to simulate embedded power electronic systems is much more efficient to simulate an average model rather that a realistic one. It takes less time, it makes it simpler, quicker and smoother, software has less computational problems and the results are accurate enough to be valid.

It's not very difficult to simulate individual components of a big electrical system: like the PV generation injecting power to the DC bus, or the VSC converter controlling the DC voltage of the LVDC distribution bus, or even the power transmission between the battery and the distribution DC bus. However, when putting all this components together to simulate the entire system, Simulink struggles and can't find the solution easily, due to different problems occurred. By the way, all the individual components are good modeled and their simulations are giving coherent and reliable results.

Another important conclusion is about the amount of solar panels needed to cover the electrical demand without additional electrical sources (the diesel generation should only be needed in case of emergency, not in normal operation). Assuming that the building has an average demand of 500kW and a peak demand of 780 kW, the approximate total area of solar panels needed to cover that demand would be higher than 2500 m^2, this amount of solar panels is probably too high to make this microgrid completely feasible in economic terms, but it is feasible in technological terms.

Let's assume that this theoretical building has a very low demand at night (because it's an office and it´s not fully operational), then the storage system should be sized in order to cover this little consume during the night, and also cover the possible irradiance irregularities during the day. The sizing of the storage system is not completely in the scope of this project, but could be an interesting way of continuing it.

6. Agraïments

Em prenc la llibertat d'escriure els agraïments en català per poder expressar-me amb total naturalitat.
Per començar, gràcies al director d'aquest treball , el professor Oriol Gomis Bellmunt. Els meus primers agraïments van dirigits a ell perquè quan li vaig comentar la meva intenció de realitzar el treball sota la seva supervisió no va dubtar ni un moment en concedir-me una reunió via Skype i, tenint en compte que jo em trobava a Holanda realitzant un programa de mobilitat, va ser molt

tranquil·litzador poder trobar un tutor per tal de realitzar un treball sobre un tema que atreia el meu interès.
També m'agradaria aprofitar per donar gràcies al departament del CITCEA en general per tres motius; donar-nos consell de forma desinteressada cada cop que ho necessitàvem, per la càlida rebuda que ens heu donat a tots els nous companys que hem estat realitzant el TFG durant aquest quadrimestre, i per la magnífica calçotada que vau organitzar a principis de Març.
En especial m'agradaria agrair a l'Eduard Prieto la seva dedicació i els seus consells. He aprés moltíssimes coses gracies a les seves llargues xerrades i explicacions. Per a ser sincer no hagués pogut realitzar aquest treball sense la seva ajuda.

7. References

[1] Luis Hernández Callejo, Yolanda Estepa Ramos, Guillermo Martínez de Lucas. Nuevo Modelo de distribución de corriente continua en baja tensión en Smart Buildings.

[2] Pasi Salonen, Tero Kaipia, Pasi Nuutinen, Pasi Peltoniemi, Jarmo Partanen. An LVDC Distribution System Concept

[3] Tero Kaipia, Pasi Salonen, Jukka Lassila, Jarmo Partanen. Possibilities of the low voltage DC distribution systems

[4] Agustí Egea Alvarez, Adrià Junyent Ferré , Oriol Gomis Bellmunt. Active and reactive power control of grid connected distributed generation systems.

[5] Samer Said, Ahmed Massoud, Mohieddine Benammar, Shehab Ahmed. A Matlab/Simulink-Based Photovoltaic Array Model Employing SimPowerSystems Toolbox

[6] M. Mikati, M. Santos, C. Armenta. Modelado y Simulación de un Sistema Conjunto de Energía Solar y Eólica para Analizar su Dependencia a la Red Eléctrica

[7] Oscar Sánchez Rodríguez. Modelo Simulink en sfunction de un sistema fotovoltaico compuesto por un simulador de sol, panel y conversor.

[8] Emili Lupon. Electrònica. Grau en Enginyeria de Tecnologies Industrials, ETSEIB

[9] Jiuchun Jiang, Yan Bao, Le Yi Wang. Topology of a Bidirectional Converter for Energy Interaction between Electric Vehicles and the Grid

[10] Mathworks.com